Background solutions to the Hubble tension in $f(Q)$ gravity and consistency with BAO measurements

José Antonio Nájera ,* Indranil Banik ,† and Harry Desmond ‡
Institute of Cosmology & Gravitation, University of Portsmouth, Dennis Sciama Building, Portsmouth, PO1 3FX, UK

Vasileios Kalaitzidis§
Scottish Universities Physics Alliance, University of Saint Andrews, North Haugh, Saint Andrews, Fife KY16 9SS, UK

(Dated: October 27, 2025)

We test whether $f(Q)$ symmetric teleparallel theories of gravity are capable of solving the Hubble tension while producing consistency with DESI DR2 BAO. We consider three different forms for the $f(Q)$ function: logarithmic, exponential, and hyperbolic tangent. We also consider extensions of these models by adding the Cosmological constant, and compare to phenomenological models with a flexible double exponential addition to the standard ΛCDM $H(z)$. We test these models against DESI DR2 BAO, *Planck* 2018, Local H_0, and Cosmic Chronometers data. The logarithmic and hyperbolic tangent models do not provide an adequate solution, while the exponential model gives a reasonable solution, though it faces mild tension with the BAO data. The models assisted by the cosmological constant perform slightly better than the exponential, at the cost of reduced theoretical motivation. This highlights the difficulties of finding a theoretically motivated solution to the Hubble tension while producing BAO consistency. The phenomenological models are able to achieve a good fit to all data, giving guidelines for what a background solution to the Hubble tension would look like in general.

I. INTRODUCTION

If General Relativity [GR; 1] is valid on cosmological scales, the matter content of the Universe must be dominated by non-baryonic cold dark matter (CDM) particles outside the standard model of particle physics, while the matter-energy content must be dominated by a cosmological constant (Λ), leading to the well-known ΛCDM paradigm [2, 3]. Its free parameters can be calibrated using the observed anisotropies in the power spectrum of the cosmic microwave background (CMB), relic radiation from redshift $z = 1090$ [4]. One of the model parameters is H_0, the present value of the Hubble parameter $H \equiv \dot{a}/a$, where a is the cosmic scale factor normalised to unity today, 0 subscripts denote present values, and an overdot denotes a time derivative. The ΛCDM prediction for H_0 based on the CMB anisotropies measured by the *Planck* satellite, the Atacama Cosmology Telescope (ACT), and the South Pole Telescope (SPT) is 67.24 ± 0.35 km/s/Mpc [4–6]. This can be tested by measuring $z' \equiv dz/dr$, the local gradient of redshift with respect to distance. In a homogeneously expanding universe, we expect that $cz' = H_0$ [section 1 of 7]. However, local measurements of cz' by several different teams using a wide variety of techniques, instruments, and tracers consistently indicate a value around 9% above that expected in ΛCDM [8, and references therein].

ΛCDM also faces another tension from the observed angular scale and redshift depth of the baryon acoustic oscillation (BAO) ruler. This is a feature in the large-scale correlation function of galaxies that was imprinted at early times, essentially corresponding to the first angular peak in the CMB power spectrum [9]. The comoving length r_d of the BAO ruler should have remained constant for $z \lesssim 1060$. Starting with the seminal works of **(author?)** [10] and **(author?)** [11], the BAO feature has been detected at increasingly higher precision, most recently by the Dark Energy Spectroscopic Instrument (DESI) Collaboration in their Data Release 2 (DR2) [12]. The measurements are in $\approx 3\sigma$ tension with ΛCDM expectations [5]. However, a look at all available BAO measurements over the last 20 years shows that the actual level of tension is more like 3.8σ, highlighting that the BAO 'anomaly' has to be taken seriously [table 2 of 13].

These difficulties with ΛCDM might suggest a problem with our understanding of the $\mathcal{O}\left(10^{-5}\right)$ CMB anisotropies. However, we can infer H_0 using only the CMB monopole temperature in combination with the primordial light element abundances, relying on the well-established theory of Big Bang nucleosynthesis [BBN; 14]. This BAO + BBN route

* antonio.najera@port.ac.uk
† indranil.banik@port.ac.uk
‡ harry.desmond@port.ac.uk
§ vk44@st-andrews.ac.uk

to H_0 gives 68.51 ± 0.58 km/s/Mpc [12], far below local measurements of cz'. Thus, problems with measurements of the subtle CMB anisotropies cannot account for the Hubble tension.

The above argument relies on ΛCDM applying prior to recombination, but if there are actually significant deviations from it, then we may be able to fit the CMB anisotropies and BBN with a higher H_0 consistent with the local cz'. There have been several proposals along these lines, for instance using primordial magnetic fields modifying the redshift of recombination [15]. However, there are at least seven serious difficulties faced by such early-time solutions to the Hubble tension [16]. One such difficulty is that the age of the Universe would be reduced by a higher expansion rate than the *Planck* cosmology for nearly the entirety of cosmic history. However, this prediction is in significant tension with observations of the oldest Galactic stars and globular clusters [17, 18], which are more in line with the *Planck* H_0 given the constraint on the matter density parameter $\Omega_{\rm M}$ from uncalibrated BAO data [19]. Another issue is that the CMB contains a wealth of detail beyond merely the angular scale of the first acoustic peak. This makes it challenging to understand the excellent fit to the CMB power spectrum in ΛCDM if there were indeed substantial deviations from it in the pre-recombination Universe [5, 6]. Another issue is that the BAO anomaly is not present at high z but grows as we get to lower $z \lesssim 1$. This trend cannot be understood through a simple recalibration of r_d, which would uniformly scale the BAO angular scale and redshift depth at any z by the same factor at all z.

These difficulties faced by ΛCDM and modifications to it at early times motivate us to consider other theories with a different late-time expansion history. Sticking to ΛCDM behaviour in the early universe would preserve the excellent fit to the CMB anisotropies in ΛCDM, provided the comoving matter density and the comoving distance to recombination remain the same as in the *Planck* cosmology. However, this leaves significant flexibility in the late-time expansion history, possibly allowing us to solve the Hubble and BAO tensions. To modify the expansion history, we need to alter either the matter-energy content of the universe or the law of gravity. In the former approach, we can introduce dynamical dark energy, where we let the dark energy Equation of State (EoS) change with redshift. However, this proposal does not explain what dark energy is, so it just provides a phenomenological approach without theoretical grounds. The latter approach is through modified theories of gravity. In this context, the late time accelerated expansion of the Universe is described via its geometry. This provides a compelling explanation for the nature of dark energy.

In this paper, we focus on this latter approach, i.e., the modified gravity formalism. Specifically, we work in the symmetric teleparallel framework, where curvature and torsion are zero and gravity is driven by non-metricity (the covariant derivative of the metric) [20]. In this background, it is possible to build the so-called *symmetric teleparallel equivalent of General Relativity (STEGR)* [21] given by the Lagrangian $\mathcal{L} = Q/(8\pi G)$. Similarly to Riemannian geometry where we can promote $R \to f(R)$ [22], we can generalize the Lagrangian to a general function of the non-metricity scalar $Q \to f(Q)$ [23]. This gives us a set of theories called $f(Q)$ gravity.

There have been numerous recent studies on $f(Q)$ gravity. The background cosmology and first order perturbations were studied in [24]. The theory was tested with redshift space distortions (RSD) in [25]. There are also studies in cosmography [26], energy conditions [27], and quantum cosmology [28]. The most general connection for the symmetric teleparallel framework was proposed in [29, 30]. Different possible functional forms for $f(Q)$ have been considered which describe an accelerated expansion of the Universe at late times and are possible alternatives to ΛCDM, for instance, power law [31], exponential [32], logarithmic [33], and hyperbolic tangent [34]. The propagation of gravitational waves in $f(Q)$ gravity has been considered in [33, 35–37]. Solar system tests for $f(Q)$ gravity were done in [38]. Some studies have proposed solutions to the Hubble tension within $f(Q)$ gravity [39–41].

Since $f(Q)$ models have achieved some observational success as previously described, it is natural to consider whether they can solve recent cosmological tensions. In the present paper, we focus on testing whether $f(Q)$ gravity models can solve the Hubble tension and at the same time achieve BAO consistency. We work with DESI DR2 data [12], *Planck* 2018 constraints [4], local H_0 measurements like SH0ES [42], and Cosmic Chronometers (or Clocks). These data help to see whether $f(Q)$ gravity is capable of solving the tensions in cosmology.

The structure of this paper is as follows. In section II, we present the theoretical formalism for $f(Q)$ gravity. Section III presents the specific models we consider. We describe the observational data used to constrain the models in section IV. We present our findings in section V and discuss their implications in section VI. We conclude in section VII. In Appendix A, we present some figures comparing the models to all available BAO data over the last twenty years.

II. $f(Q)$ GRAVITY THEORY

Gravity is a geometrical entity that is usually built upon Riemannian Geometry, where the only non-vanishing quantity is the Riemann tensor $R^{\alpha}{}_{\beta\mu\nu}$. The standard ΛCDM cosmological model was proposed within this formalism. However, the most general type of geometry is called *metric-affine geometry* consisting of a triple $(\mathcal{M}, g, \Gamma)$ [43]. For this, we need to choose a manifold $\mathcal{M}$, a metric g, and a connection Γ. Given a connection, there is a notion of parallel transport. Its effects on vectors can be quantified by three tensors. The Riemann tensor $R^{\alpha}{}_{\beta\mu\nu}$ quantifies how a vector changes its direction when moved on an infinitesimal closed path. We now consider two infinitesimal direction vectors δv_a, δv_b and we perform a parallel transport first along δv_a and then along δv_b. The torsion tensor $T^{\alpha}{}_{\mu\nu}$ quantifies the difference in parallel transport from this operation and the parallel transport along δv_b first and then δv_a. Thus, torsion quantifies how the parallelogram is no longer closed by changing the order of parallel transport [44]. Finally, the non-metricity tensor $Q_{\alpha\mu\nu}$ quantifies the change in a vector's length when comparing it at two infinitesimally close points p and q [45].

The most general connection includes the Levi-Civita standard connection, plus terms of the torsion and non-metricity tensors [44, 45]. We are free to make restrictions to the connection. Thus, we can set one or two of the three fundamental tensors to zero. There are in fact two equivalent ways of building GR in flat spacetime, which alongside GR leads to the geometric trinity of gravity [21]. We have the Teleparallel Equivalent of General Relativity (TEGR) where we set the Riemann and non-metricity tensors to zero and gravity is driven by torsion [46]. On the other hand, if we set the Riemann and torsion tensors to zero, we get the STEGR [20]. There is no observational difference between the three cases. However, their theoretical construction is quite different, as it completely changes how parallel transport works. By generalizing the GR Lagrangian, for instance by promoting $R \to f(R)$, we build a new set of theories where we have arbitrary functions of the Ricci scalar [22]. Similarly, we can build $f(T)$ [47] and $f(Q)$ [23] theories by having arbitrary functions of the torsion and non-metricity scalars, respectively. In the present paper, we focus on the latter formalism, called *symmetric teleparallel gravity*. Symmetric means the connection is symmetric in its lower indices, while teleparallel means the curvature is zero.

The fundamental tensor in symmetric teleparallelism is the non-metricity tensor, which is given by the covariant derivative of the metric

$$Q_{\alpha\mu\nu} \equiv \nabla_\alpha g_{\mu\nu}, \tag{1}$$

and from this, we can derive several tensors called the disformation and superpotential [23, 24].

$$L^{\alpha}{}_{\mu\nu} = \frac{1}{2} Q^{\alpha}{}_{\mu\nu} - Q_{(\mu}{}^{\alpha}{}_{\nu)}, \tag{2}$$

$$P^{\alpha}{}_{\mu\nu} = -\frac{1}{2} L^{\alpha}{}_{\mu\nu} + \frac{1}{4}(Q^\alpha - \tilde{Q}^\alpha) g_{\mu\nu} - \frac{1}{4}\delta^{\alpha}_{(\mu} Q_{\nu)}, \tag{3}$$

where $Q_\alpha = g^{\mu\nu} Q_{\alpha\mu\nu}$ and $\tilde{Q}_\alpha = g^{\mu\nu} Q_{\mu\alpha\nu}$. Finally, the non-metricity scalar is [23, 24]

$$Q = -Q_{\alpha\mu\nu} P^{\alpha\mu\nu} = -\frac{1}{4}(-Q^{\alpha\mu\nu} Q_{\alpha\mu\nu} + 2Q^{\alpha\mu\nu} Q_{\nu\alpha\mu} - 2Q^\alpha \tilde{Q}_\alpha + Q^\alpha Q_\alpha), \tag{4}$$

so the non-metricity scalar is given by four traces of the non-metricity tensor. We can now consider the general action

$$S = \int d^4x \sqrt{-g} \left(-\frac{1}{2} f(Q) + \mathcal{L}_m \right), \tag{5}$$

where g is the determinant of the metric, $f(Q)$ is a function of the non-metricity scalar and $\mathcal{L}_m$ is the matter Lagrangian. STEGR takes the form $f(Q) = Q/(8\pi G)$ [23]. By taking the variation δS with respect to the metric ($\delta S/\delta g^{\mu\nu}$) and setting it to zero, we derive the field equations [23]

$$\frac{2}{\sqrt{-g}} \nabla_\alpha \left[\sqrt{-g} P^{\alpha}{}_{\mu\nu} f_Q \right] + f_Q q_{\mu\nu} - \frac{1}{2} f g_{\mu\nu} = T_{\mu\nu}, \tag{6}$$

where $f_Q = df/dQ$ and

$$q_{\mu\nu} = P_{(\mu|\alpha\beta} Q_{\nu)}{}^{\alpha\beta} - 2P^{\alpha\beta}_{(\nu} Q_{\alpha\beta|\mu)}. \tag{7}$$

Finally, by taking $\delta S/\delta \Gamma^{\alpha}{}_{\mu\nu} = 0$, we get [23]

$$\nabla_\mu \nabla_\nu (\sqrt{-g} f_Q P^{\mu\nu}{}_\alpha) = 0. \tag{8}$$

To derive the modified Friedmann equations, we start from the flat Friedmann-Lemaitre-Robertson-Walker (FLRW) metric

$$ds^2 = -dt^2 + a^2(t) \delta_{ij} dx^i dx^j, \tag{9}$$

with $a(t)$ the scale factor normalised to unity today. In this case, we are setting the lapse function $N(t) = 1$. From a general lapse function, we can always take the time reparametrization $t = \int_0^t d\tau \sqrt{-g_{tt}(\tau)}$, i.e., the lapse function is unphysical [29]. The remaining ingredient to derive the Friedmann equations is the connection. The most general connection for a flat spacetime in the symmetric teleparallel framework is given by [29, 30]

$$\Gamma^t{}_{\mu\nu} = \begin{pmatrix} C_1 & 0 & 0 & 0 \\ 0 & C_2 & 0 & 0 \\ 0 & 0 & C_2 r^2 & 0 \\ 0 & 0 & 0 & C_2 r^2 \sin\theta \end{pmatrix}, \tag{10}$$

$$\Gamma^r_{\mu\nu} = \begin{pmatrix} 0 & C_3 & 0 & 0 \\ C_3 & 0 & 0 & 0 \\ 0 & 0 & -r & 0 \\ 0 & 0 & 0 & -r\sin^2\theta \end{pmatrix}, \tag{11}$$

$$\Gamma^\theta{}_{\mu\nu} = \begin{pmatrix} 0 & 0 & C_3 & 0 \\ 0 & 0 & \frac{1}{r} & 0 \\ C_3 & \frac{1}{r} & 0 & 0 \\ 0 & 0 & 0 & -\cos\theta\sin\theta \end{pmatrix}, \tag{12}$$

$$\Gamma^\phi{}_{\mu\nu} = \begin{pmatrix} 0 & 0 & 0 & C_3 \\ 0 & 0 & 0 & \frac{1}{r} \\ 0 & 0 & 0 & \cot\theta \\ C_3 & \frac{1}{r} & \cot\theta & 0 \end{pmatrix}, \tag{13}$$

where $C_1(t)$, $C_2(t)$, and $C_3(t)$ are functions of time. There are three different possible forms for these functions that satisfy spatial flatness in the symmetric teleparallel framework. These are [29]:

1. Connection I: $C_1(t) = C_3(t) + \dfrac{\dot{C}_3(t)}{C_3(t)}, C_2(t) = 0$.
2. Connection II: $C_1 = -\dfrac{\dot{C}_2(t)}{C_2(t)}, C_3(t) = 0$.
3. Connection III: $C_2(t) = C_3(t) = 0$.

Connection III is the simplest as the function $C_1(t)$ does not appear in the modified Friedmann equations and it is undetermined by them [29]. Furthermore, by setting $C_1(t) = 0$, we recover the so-called *coincident* gauge, where the connection vanishes and the covariant derivatives become partial derivatives [23]. Connections I and II allow for an additional degree of freedom that changes the dynamics of the Hubble factor. For example, different connections imply different cosmological constraints [48] and different potential stability concerns [49]. Furthermore, different connections can resolve cosmological singularities like the Big Bang and Big Rip, replacing them with smooth de-Sitter phases [50]. Therefore, considering different connections gives more flexibility to $f(Q)$ gravity models, with the potential of alleviating or solving problems in cosmology like the Hubble and BAO tensions.

In this paper, we will work with Connection III as it is the one that has been studied the most. This will provide insights on the capabilities of $f(Q)$ gravity to solve the Hubble tension without the flexibility of an extra degree of freedom. Future work might consider alleviating the Hubble tension within $f(Q)$ with the assistance of a connection degree of freedom that can increase the accelerated expansion at late times and simultaneously fit the BAO data.

By using Connection III and considering a perfect fluid with density ρ and pressure p, the modified Friedmann equations are

$$Qf_Q - \frac{1}{2}f = \rho, \tag{14}$$

$$(2Qf_{QQ} + f_Q)\dot{H} = -\frac{1}{2}(\rho + p), \tag{15}$$

$$Q = 6H^2, \tag{16}$$

$$\dot{\rho} + 3H(\rho + p) = 0, \tag{17}$$

where $H(z)$ is the Hubble factor. By using the STEGR form $f(Q) = Q/(8\pi G)$, we recover the standard Friedmann equations. If we add the standard Friedmann equations, we can separate the density and pressure contributions from the effective $f(Q)$ gravity contributions. This allows us to derive the effective $f(Q)$ equation of state

$$w_{f(Q)} = \left(\frac{\kappa p(1 - \tilde{f}_Q - 12H^2\tilde{f}_{QQ}) + 3H^2\tilde{f}_Q - 36H^4\tilde{f}_{QQ} - \frac{1}{2}\tilde{f}}{\tilde{f}_Q + 12H^2\tilde{f}_{QQ}} \right) \left(\frac{2\tilde{f}_Q}{\frac{1}{2}\tilde{f} + \kappa\rho(1 - 2\tilde{f}_Q)} \right), \tag{18}$$

where $\kappa \equiv 8\pi G$, $f \equiv \tilde{f}/\kappa$, $f_Q \equiv \tilde{f}_Q/\kappa$ and $f_{QQ} \equiv \tilde{f}_{QQ}/\kappa$. This expression is useful to determine whether the effective $f(Q)$ dark energy has quintessence, cosmological constant, phantom, or phantom crossing behaviour.

III. SPECIFIC $f(Q)$ MODELS

In this section, we present the models we study. The goal is to see if they can solve the Hubble tension and achieve consistency with the DESI DR2 BAO data [12]. This is important as doing both is difficult for a cosmological model. For example, the Chevallier-Polarski-Linder [CPL; 51–53] w_0w_a parametrization is preferred over ΛCDM at the 3.1σ C.L. using DESI DR2 and CMB data [12]. However, the predicted value for the Hubble constant is $H_0 = 63.9^{+1.7}_{-2.1}$ km/s/Mpc using CMB + DESI DR2 [15]. This is in 4.86σ tension with the latest independent H_0 determination using Cepheid-Type Ia supernovae by the SH0ES Collaboration [54]. Therefore, the main goal of this paper is to determine whether modified $f(Q)$ gravity models can solve the Hubble tension without losing consistency with BAO data. We explore three models previously studied in the literature that geometrically imply an accelerated expansion of the universe and include additional terms that can increase $H(z)$ at late times. A recent study [41] went along these lines by considering a power-law hyperbolic tangent $f(Q)$ model. They found that the model alleviates the Hubble tension using DESI + RSD + Cosmic Chronometers (CC) + Standard Sirens + CMB data.

A. Logarithmic $f(Q)$ Model ("Log")

First, we propose a logarithmic model of the form [33]

$$f(Q) = \frac{Q}{8\pi G} - \alpha \ln\left(\frac{Q}{Q_0}\right), \tag{19}$$

with $Q_0 \equiv Q(z = 0)$. This model predicts accelerated expansion consistently with SNIa and BAO data [33]. The Friedmann equation for $E \equiv H/H_0$ is given by [33]

$$E^2 + \Omega_\alpha \ln E = \Omega_\alpha + \Omega_m(1 + z)^3, \tag{20}$$

where $\Omega_\alpha = (8\pi G\alpha)/(3H_0^2)$ is an effective geometric density. The closure relation gives

$$\Omega_m + \Omega_\alpha = 1, \tag{21}$$

which has the same number of parameters as ΛCDM. As we can see, the Friedmann equation is the ΛCDM one apart from a logarithmic correction to the left-hand side. When $z \gg 1$, this term is much smaller than E^2, making the behaviour the same as ΛCDM at high z. However, at low z, the logarithmic term makes an additional contribution that can enhance the late-time accelerated expansion.

B. Exponential $f(Q)$ Model ("Exp")

Next we consider an exponential model of the form [32]

$$f(Q) = \frac{Q}{8\pi G} \exp\left(\frac{\lambda Q_0}{Q}\right). \tag{22}$$

This was also the first $f(Q)$ model that could challenge ΛCDM statistically [32]. The Friedmann equation is

$$(E^2 - 2\lambda) \exp\left(\frac{\lambda}{E^2}\right) = \Omega_m (1+z)^3, \tag{23}$$

and the closure relation gives a solution for the λ parameter

$$\lambda = \frac{1}{2} + \mathcal{W}_0\left(-\frac{\Omega_m}{2\sqrt{e}}\right), \tag{24}$$

where $\mathcal{W}_0$ is the principal branch of the Lambert function. Therefore, this function also has the same number of parameters as ΛCDM. In this case, the modified Friedmann equation provides an exponential term that scales like E^{-2}. When $E^2 \gg \lambda$, then $E^2 \sim \Omega_m(1+z)^3 - \lambda$, having a behaviour like ΛCDM but with an exponential correction at low redshift.

C. Hyperbolic Tangent $f(Q)$ Model ("Tanh")

Finally, we consider a third $f(Q)$ model given by [34]

$$f(Q) = \frac{Q}{8\pi G} + \alpha \tanh\left(\frac{Q_0}{Q}\right), \tag{25}$$

where the component causing a higher accelerated expansion comes from the hyperbolic tangent term. The Friedmann equation is

$$E^2 - \frac{\Omega_\alpha}{E^2}\left(\cosh^{-2}\left(E^{-2}\right)\right) - \frac{1}{2}\Omega_\alpha \tanh(E^{-2}) = \Omega_m(1+z)^3, \tag{26}$$

where $\Omega_\alpha = (8\pi G\alpha)/(3H_0^2)$, like in the logarithmic model. The closure equation gives

$$\Omega_m + \Omega_\alpha\left(\cosh^{-2}(1) + \frac{1}{2}\tanh(1)\right) = 1, \tag{27}$$

which again has the same number of parameters as ΛCDM.

D. Including a Cosmological Constant

In $f(Q)$ gravity, the late-time accelerated expansion of the Universe can arise purely from geometric effects, without the need for an exotic dark energy component [27, 55]. The nonlinear dependence of the action on the non-metricity scalar Q introduces effective gravitational terms that behave as a fluid with negative pressure. When these geometric contributions are moved to the right-hand side of the field equations, they form an effective energy–momentum tensor with $\rho_{\rm eff} + 3p_{\rm eff} < 0$, corresponding to an effective equation-of-state parameter $w_{\rm eff} = p_{\rm eff}/\rho_{\rm eff} < -1/3$. This violation of the strong energy condition allows gravity to act repulsively and drive the observed cosmic acceleration. At the same time, viable $f(Q)$ models typically satisfy the weak and dominant energy conditions, $\rho_{\rm eff} > 0$, $\rho_{\rm eff} + p_{\rm eff} > 0$, and $\rho_{\rm eff} \geq |p_{\rm eff}|$, ensuring positive energy density, physically well-behaved matter, and causal (subluminal) energy flow. Thus, $f(Q)$ gravity provides a geometric explanation for cosmic acceleration while maintaining physically reasonable energy and causality properties [55].

Despite the cosmological constant not being necessary to produce accelerated expansion in $f(Q)$ gravity, we also consider models in which it is included to gauge its effect on the Hubble and BAO tensions. This is achieved by

TABLE I. Summary of the observational data considered in this paper.

Data	Description	References
Local H_0	Four model independent local H_0 determinations	[54, 57–59]
DESI DR2 BAO	The most recent BAO measurements from the DESI collaboration	[12]
Cosmic Chronometers	32 $H(z)$ measurements using the differential age method	[60]
Planck 2018 constraints	TT, TE, EE + lowE constraints for $\Omega_m h^2$ and the comoving distance to recombination	[4]

adding $\Lambda/(4\pi G)$ to the $f(Q)$ function. The Friedmann equations get an additional Ω_Λ term on the right-hand side, while the closure relations get this term on the left-hand side. For the exponential model, the solution for λ is now

$$\lambda = \frac{1}{2} + \mathcal{W}_0\left(-\frac{\Omega_m + \Omega_\Lambda}{2\sqrt{e}}\right). \tag{28}$$

These variations have one more free parameter than ΛCDM. The new free parameter allows for extra flexibility in the Hubble parameter that might enhance the agreement with BAO. The drawback is that by adding the cosmological constant these models will only explain part of dark energy geometrically, undermining their theoretical motivation. We refer to these variants in the remainder of the paper as Log + Λ, Exp + Λ, and Tanh + Λ.

E. Phenomenological Model (Phen)

In addition to the $f(Q)$ models, we propose a flexible phenomenological model to study whether it is possible to solve the Hubble constant tension and BAO anomalies at the background level, and if so what form such a solution would take. The proposed model is

$$H(z) = H_{0\Lambda CDM}\sqrt{\Omega_m(1+z)^3 + 1 - \Omega_m} + A\exp(-z/z_1) + B[\exp(-z/z_1) - \exp(-z/z_2)], \tag{29}$$

with $z_2 \equiv kz_1$. This model has six free parameters, with the A exponential term introducing a correction that allows for faster accelerated expansion at late-times. The measured Hubble constant would be $H_0 = H_{0\Lambda CDM} + A$. The B term is designed to compensate a higher $H(z)$ at low z with a lower $H(z)$ at high z, allowing models with $A > 0$ to preserve the comoving distance to recombination and thereby retain consistency with the CMB.

IV. OBSERVATIONAL DATA

We constrain the parameter vector $\Theta = \{\Omega_m, H_0\}$ for the $f(Q)$ models, $\Theta = \{\Omega_m, \Omega_\Lambda, H_0\}$ for the cosmological constant variants, and $\Theta = \{\Omega_m, H_0, A, B, z_1, k\}$ for the phenomenological model. Since we are focusing on late-time solutions without changing the physics at early times, we treat r_d as an additional parameter with a Gaussian prior of $r_d = 147.05 \pm 0.30$ Mpc, which is the *Planck* 2018 TT,TE,EE+lowE constraint [4]. This parameter is tightly constrained by its prior, so we do not report posteriors for it but simply marginalise over it. For the latter, we consider three cases ($k = 2$, $k = 3$, k free). To determine if the $f(Q)$ models can alleviate or solve the Hubble tension and BAO anomalies, we use four of the latest independent H_0 constraints, the latest BAO DESI DR2 [12], and the $H(z)$ measurements obtained with the CC method [56, and references therein]. Finally, we use the constraints for the physical density parameter $\Omega_m h^2$ and the comoving distance to recombination from $100\,\theta_\star$. *Planck* 2018 gives very strong, so if we want a solution to the Hubble tension, we need to either fit the *Planck* 2018 constraints and solve the tension at late times, or use early time physics. The latter implies the age of the universe $\propto H_0^{-1}$, reducing its predicted age and causing additional complications fitting the CMB data [5, 6, 16]. In the present paper, we choose the former approach and thus impose the *Planck* 2018 constraints on the cosmological parameters. We summarize the observational data in Table I. We note that if the matter density at any z and the comoving distance to recombination are the same as in the *Planck* ΛCDM cosmology, there should be no difficulty fitting the CMB anisotropies given the lack of new physics at early times.

A. Model Independent H_0 Determinations

We use four recent model-independent H_0 constraints: the latest SH0ES constraint using the Small Magellanic Cloud as an extra anchor [54], the result from the Megamaser Cosmology project using only geometric distances [57], the result from the TRGB-SBF project using neither Cepheids nor supernovae [58], and a one-step (or rung-free) determination using Type II supernovae [59].

1. SH0ES

The Supernova H_0 for the Equation of State (SH0ES) collaboration provides the most precise model-independent determination of the Hubble constant. This uses a three rung cosmic distance ladder with geometric distances calibrating the Period-Luminosity relation of Cepheid variable stars [the Leavitt Law; 61]. The second rung uses this relation to determine the absolute magnitude of SNIa. Finally, the third rung uses SNIa in the Hubble flow with $z = 0.023 - 0.15$ to obtain that $H_0 = 73.17 \pm 0.86$ km/s/Mpc [54]. This is in 5.8σ tension with the CMB flat ΛCDM constraint from *Planck* 2018 [$H_0 = 67.36 \pm 0.54$ km/s/Mpc; 4]. The discrepancy can be due to unaccounted-for systematics in the SH0ES Cepheids-SNIa distance ladder, though the good agreement with a number of other techniques argues against this interpretation [8, and references therein]. The other possibility is new physics in the form of an extension to ΛCDM.

The phenomenological models have a caveat that needs to be handled for this H_0 constraint. SH0ES computes H_0 by fitting $H(z)$ with a Taylor series (the cosmographic expansion). If $z_1 \lesssim 0.15$ and thus lies within the SH0ES redshift range, the predicted $H(z)$ for the phenomenological models will strongly curve in the SH0ES redshift. The phenomenological model prediction for H_0 will then not correspond to what we would infer from the SH0ES distance ladder. Thus, for the phenomenological models, we compute the predicted $H(z)$ for all redshifts inside the third rung of the distance ladder. We fit the second-order cosmographic expansion using $q_0 = -0.55$, the value considered by SH0ES [42, 54]. The extrapolated $H(z = 0)$ of our cosmographic expansion is then compared with SH0ES. This makes our analysis more realistic by predicting the H_0 we would derive in the model from the SH0ES distance ladder approach. For simplicity, we neglect the third order jerk parameter due to the low redshifts involved. We note that our other models lack sharp features in the predicted $H(z)$ at low z, so this complication does not arise.

2. Megamaser Cosmology Project

This is an independent determination of H_0 using geometric parallaxes to measure the distance modulus to megamaser host galaxies. It combines six host galaxies (UGC 3789, NGC 6264, NGC 6323, NGC 5765b, CGCG 074-064 and NGC 4258), giving a final result of $H_0 = 73.9 \pm 3.0$ km/s/Mpc [57]. This estimate exceeds *Planck* 2018 by 2.15σ and SH0ES by only 0.23σ.

3. TRGB-SBF Project

The third H_0 measurement we consider is the one given by the TRGB-SBF project [58]. This is a three rung distance ladder like SH0ES. However, the second rung calibrator is the Tip of the Red Giant Branch (TRGB) instead of Cepheids. Finally, the third rung uses Surface Brightness Fluctuations (SBF) instead of SNIa. This provides an independent determination of $H_0 = 73.8 \pm 2.4$ km/s/Mpc [58], which exceeds *Planck* 2018 by 2.62σ and SH0ES by only 0.25σ.

4. Type II SN H_0

The fourth and final H_0 independent constraint we consider is a new determination using no rungs. This comes from spectral modelling of Type II supernovae. Using the tailored expanding photosphere method for Type II SN, the H_0 constraint is 74.9 ± 1.9 km/s/Mpc [59]. The systematic uncertainty is comparable to or less than the statistical uncertainty [59]. To be conservative, we consider the systematic uncertainty to equal the statistical one, giving a value of $H_0 = 74.9 \pm 2.7$ km/s/Mpc. This determination is 2.74σ above *Planck* 2018 and 0.61σ above SH0ES.

5. H_0 determinations likelihood

We model each of the H_0 constraints above as Gaussian likelihood terms:

$$\log \mathcal{L}_{H_0} = -\frac{1}{2} \sum_{i=1}^{4} \log\left(2\pi\sigma_{H_{0,i}}^2\right) - \frac{1}{2} \sum_{i=1}^{4} \left(\frac{H_0 - H_{0,i}}{\sigma_{H_{0,i}}}\right)^2, \tag{30}$$

where $H_{0,i}$ is the i-th H_0 determination and $\sigma_{H_{0,i}}$ its 1σ C.L. uncertainty. We are including the χ^2 term and the normalisation for a computation of the Bayesian evidence. The i index runs over the four H_0 independent measurements considered. These measurements have been chosen to be as independent as possible, as we are assuming by summing the log-likelihoods. The Type II SN constraint is fully independent of the others. There is a small covariance between the Megamaser determination with SH0ES and the TRGB-SBF project because the latter two use the NGC 4258 megamaser as a calibrator for Cepheids and the TRGB, but we neglect this for simplicity. SH0ES and TRGB-SBF are fully independent since they use different calibrators (Cepheids vs TRGB) and distance indicators in the Hubble flow (SNIa vs SBF).

B. DESI DR2 BAO

Baryon Acoustic Oscillations (BAOs) are fluctuations of the baryonic matter that act as a standard ruler. We include the measurements from the latest release by the Dark Energy Spectroscopic Instrument (DESI) [12]. Their DR2 provides six measurements of D_H/r_d, six of D_M/r_d, and one of D_V/r_d, where

$$D_H(z) = \frac{c}{H(z)}, \tag{31}$$

$$D_M(z) = c\int_0^z \frac{dz'}{H(z')}, \tag{32}$$

$$D_V(z) \equiv (zD_M^2(z)D_H)^{1/3}. \tag{33}$$

The sound horizon is

$$r_d = \int_{z_d}^{\infty} dz' \frac{c_s(z')}{H(z')}, \tag{34}$$

where c_s is the sound speed. We are interested in studying late time solutions to the Hubble tension, without introducing new physics at early times. Thus, we will take the standard *Planck* 2018 TT,TE,EE+lowE constraint that $r_d = 147.05 \pm 0.30$ Mpc [4]. The logarithmic likelihood for this is given by

$$\log \mathcal{L}_{\rm DESI\ DR2} = -\frac{1}{2}\log(2\pi|C_{\rm DESI\ DR2}|) - \frac{1}{2}\Delta G(z,\Theta)^T C^{-1}_{\rm DESI\ DR2}\Delta G(z,\Theta), \tag{35}$$

where $C_{\rm DESI\ DR2}$ is the covariance matrix of the data and $\Delta G(z,\Theta) = G(z,\Theta) - G_{\rm DESI\ DR2}(z)$. G includes the 13 DESI DR2 measurements. However, for a visual representation of the agreement or tension of the models with BAO data, we also show BAO data from the last 20 years (table 1 in [13]).

C. Cosmic Chronometers (CC)

We consider the CC compilation presented in [56]. This includes 32 $H(z)$ measurements. By considering an FLRW universe, we can write the Hubble factor as

$$H(z) = -\frac{\dot{z}}{1+z}. \tag{36}$$

$\dot{z}$ can be measured with the differential age evolution of early-type galaxies [62]. This provides model-independent measurements of the Hubble factor. The logarithmic CC likelihood is

$$\log \mathcal{L}_{CC} = -\frac{1}{2}\sum_{i=1}^{32}\log(2\pi\sigma^2_{CC,\,i}) - \frac{1}{2}\sum_{i=1}^{32}\left(\frac{H(z_i,\Theta) - H_{CC}(z_i)}{\sigma_{CC,\,i}}\right)^2, \tag{37}$$

where $H(z_i,\Theta)$ is the predicted theoretical Hubble factor, $H_{CC}(z_i)$ the observed Hubble factor from CC, and $\sigma_{CC,\,i}$ the CC 1σ C.L. uncertainty. The covariance is small for this dataset, so we neglect it.

D. *Planck* 2018 Constraints

We impose two *Planck* 2018 constraints since we are interested in late-time solutions to the Hubble constant tension. We take the TT,TE,EE+lowE constraints for $\Omega_m h^2$ and the comoving distance to recombination. By doing so, we ensure that the position and the relative heights of the CMB peaks remain unchanged. Finally, the damping tail is preserved. In particular, we consider $\Omega_m h^2 = 0.1432 \pm 0.0013$ [4]. We derive the mean value of the comoving distance to recombination by taking the integral

$$D_M(z_\star) = c \int_0^{z_\star} \frac{dz}{H(z)}, \tag{38}$$

where c is the speed of light and $z_\star$ is the redshift at recombination. We neglect radiation for simplicity, giving $H(z) = H_0\sqrt{\Omega_m(1+z)^3 + 1 - \Omega_m}$. We take the *Planck* 2018 TT,TE,EE+lowE constraints for $H_0, \Omega_m, z_\star$. For the 1σ C.L. error, we combine in quadrature the *Planck* 2018 percentage error for the recombination angle $\theta_\star$ and the sound horizon to recombination $r_\star$.

$$\sigma_{D_M(z_\star)} = D_M(z_\star)\sqrt{\left(\frac{\sigma_{r_\star}}{r\star}\right)^2 + \left(\frac{\sigma_{\theta_\star}}{\theta_\star}\right)^2}\,, \tag{39}$$

which gives a final result of $D_M(z_\star) = 13930.72 \pm 29.22$ Mpc. The logarithmic likelihood for the *Planck* 2018 constraints is thus given by

$$\log \mathcal{L}_{\text{Planck 2018}} = -\frac{1}{2}\sum_{i=1}^{2} \log(2\pi\sigma^2_{\text{Planck 2018},i}) - \frac{1}{2}\sum_{i=1}^{2}\left(\frac{\Delta_{\text{Planck 2018},i}}{\sigma_{\text{Planck 2018},i}}\right)^2, \tag{40}$$

where $\Delta_{\text{Planck 2018},i}$ is the difference between the mean value of the *Planck* 2018 constraint and the theoretical prediction for the comoving distance to recombination or $\Omega_m h^2$, while $\sigma_{\text{Planck 2018},i}$ is the *Planck* 2018 1σ C.L. uncertainty.

V. RESULTS

We use the nested sampling algorithm `dynesty`[63] [64–68] to compute the posterior probability and the Bayesian evidence Z. We take 500 live points and use a stopping criterion of $\Delta \log \hat{Z} = 0.01$ (the hat denotes that this is not the true evidence, but the approximate remaining evidence). This tolerance is sufficient for our purposes because the different models considered have much larger evidence differences. We plot the 1σ and 2σ C.L. contours using the `GetDist`[69] package [70]. Posterior convergence was confirmed by checking that the number of effective samples was $N_{\text{eff}} > 2000$ for all models.

To determine if the theoretical models can challenge the standard ΛCDM model, we compute their logarithmic Bayes factor. This is given by

$$\log B_{PB} = \log \mathcal{E}_P - \log \mathcal{E}_B, \tag{41}$$

where P is the proposed model and B is the baseline model (ΛCDM). The Bayes factor will be negative if the ΛCDM model is preferred over the modified $f(Q)$ models, whereas the modified models are statistically preferred if the Bayes factor is positive. The strength of the preference is given by the Jeffreys criterion, as described by Kass and Raftery [71] following the convention often adopted in the cosmology literature [72]. According to this, $|\log B_{PB}| < 1$="weak evidence", $1 < |\log B_{PB}| < 3$="substantial evidence", $3 < |\log B_{PB}| < 5$="strong evidence" and $|\log B_{PB}| > 5$="very strong evidence".

Our main results are as follows:

1. We present the mean values and 1σ C.L. uncertainties for the $f(Q)$ gravity model parameters in table II and the 1σ and 2σ C.L. contours in Figure 1. We present the same results for the phenomenological models in Table III and Figure 2.

2. The predicted $\dot{a}$ as a function of redshift for all models is shown in Figure 3. We also show the ΛCDM model for comparison, visualising how the proposed models must go higher than ΛCDM at low redshift and then lower at high redshift to have the same comoving distance to recombination.

TABLE II. Mean values and 1σ C.L. uncertainties for the parameter vector $\Theta = \{\Omega_m, \Omega_\Lambda, H_0\}$ in the ΛCDM and $f(Q)$ models.

Model	Ω_m	Ω_Λ	H_0 (km/s/Mpc)
ΛCDM	0.2879 ± 0.0040	-	69.98 ± 0.37
Log	0.2775 ± 0.0036	-	72.67 ± 0.37
Log + Λ	0.2832 ± 0.0041	0.467 ± 0.084	71.02 ± 0.49
Exp	0.2750 ± 0.0038	-	72.23 ± 0.38
Exp + Λ	0.2794 ± 0.0044	$0.196^{+0.087}_{-0.11}$	71.42 ± 0.55
Tanh	0.2766 ± 0.0036	-	72.56 ± 0.37
Tanh + Λ	0.2829 ± 0.0041	0.467 ± 0.087	70.99 ± 0.49

TABLE III. Mean values and 1σ C.L. uncertainties for the parameter vector $\Theta = \{\Omega_m, H_0, A, B, z_1, k\}$ in the phenomenological models.

Model	Ω_m	H_0 (km/s/Mpc)	A	B	z_1	k
ΛCDM	0.2879 ± 0.0040	69.98 ± 0.37	-	-	-	-
Phen, k free	$0.292^{+0.011}_{-0.014}$	$74.2^{+1.0}_{-1.3}$	$4.4^{+1.5}_{-2.0}$	5^{+18}_{-24}	$0.150^{+0.029}_{-0.10}$	$1.76^{+0.29}_{-1.5}$
Phen, $k=2$	0.293 ± 0.014	74.5 ± 1.2	$4.9^{+2.0}_{-1.6}$	$8.3^{+9.5}_{-6.3}$	$0.110^{+0.030}_{-0.062}$	-
Phen, $k=3$	0.293 ± 0.016	74.4 ± 1.2	4.7 ± 2.1	$2.9^{+9.8}_{-2.8}$	$0.098^{+0.037}_{-0.094}$	-

3. We present the comparison between the isotropically averaged comoving BAO scale $\alpha_{\rm iso} = D_V/D_{V,\Lambda\rm CDM}$ for the best fits of all the models and the BAO data from the last 20 years (Ho'oleilana [73], DESI [12], SDSS [74–94], 6dFGS [75, 95], WiggleZ [96], DES [97–100], DECaLS [101]) in figure 4 (note that this is only for visual comparison, since only the DESI DR2 data was used as a BAO constraint). We present similar results for the Hubble distance ratio $\alpha_\perp = D_H/D_{H,\Lambda\rm CDM}$ and the comoving distance ratio $\alpha_\parallel = D_M/D_{M,\Lambda\rm CDM}$ in figures 6 and 7 in the appendix.

4. In figure 5, we show the $f(Q)$ effective dark energy equation of state (EoS), derived using equation (18) or $w = -(1+2/3(\dot{H}/H^2))/\Omega_{\rm DE}(z)$ (where we subtract the matter density and $\Omega_{\rm DE}(z) = 1 - \dfrac{\Omega_m(H_{0\,\Lambda\rm CDM} + A)^2(1+z)^3}{H^2}$) for the phenomenological models. We also show the cosmological constant ($+\Lambda$) behaviour for comparison.

5. We report the Bayes factor for all models with respect to ΛCDM and their predicted age of the universe t_0 (Table IV).

6. To study the agreement of each model with the data, we report the χ^2 contributions for each observational constraint (Table V). We include components for DESI DR2 BAO, independent H_0 determinations, *Planck* 2018 CMB, and CC. This helps to study the consistency between the models and the data, clarifying whether the models can solve the Hubble and BAO tensions.

As we can see in table II and figure 1, all the modified $f(Q)$ models are capable of solving (or at least significantly ameliorating) the Hubble tension by giving high values for H_0 of around 72 km/s/Mpc. However, when the cosmological constant is added, the fit to the local H_0 measurements worsens, going below 72 km/s/Mpc in all cases. Moreover, the $f(Q)$ models have a lower Ω_m to compensate for the higher H_0 and still match the *Planck* 2018 constraints. The effect of adding the cosmological constant is to lower H_0 and increase Ω_m. The phenomenological models also resolve the Hubble tension, having H_0 around 74 km/s/Mpc. Interestingly, Ω_m is higher for these models (Table III and Figure 2). The contours for the phenomenological model with k free are highly non-Gaussian, but the joint constraints on B, z_1, k are only mildly degenerate, indicating that the data is able to constrain the parameters individually. This is especially true when k is held fixed. The jaggedness of the contours with free k seems not to be caused by a convergence issue – we repeated the analysis with triple the number of live points, but this does not make the contours smooth. The number of effective samples was already > 3000.

In Figure 3, we can see that all models have $\dot{a}$ curves above ΛCDM at low redshift but below ΛCDM at higher redshift. This transition occurs at a considerably lower redshift for the phenomenological models. The $f(Q)$ models depart considerably from ΛCDM, but they converge to ΛCDM at high redshift. The $f(Q)+\Lambda$ models show a similar behaviour to each other and are closer to ΛCDM than the models not assisted by a cosmological constant.

Figure 5 shows that the Exp model has a phantom behaviour and converges to the cosmological constant both at high redshift and in the infinite future ($z \to -1$). The Tanh model has an effective phantom crossing with a quintessence behaviour at very low redshift, becoming phantom at higher redshift. The Log model has a singularity problem: it starts with phantom behaviour today, jumps to $w > -1/3$, and then becomes quintessence at high redshift. Close to $z = 2$, the effective densitychanges sign, but the pressure stays negative. This creates a singularity

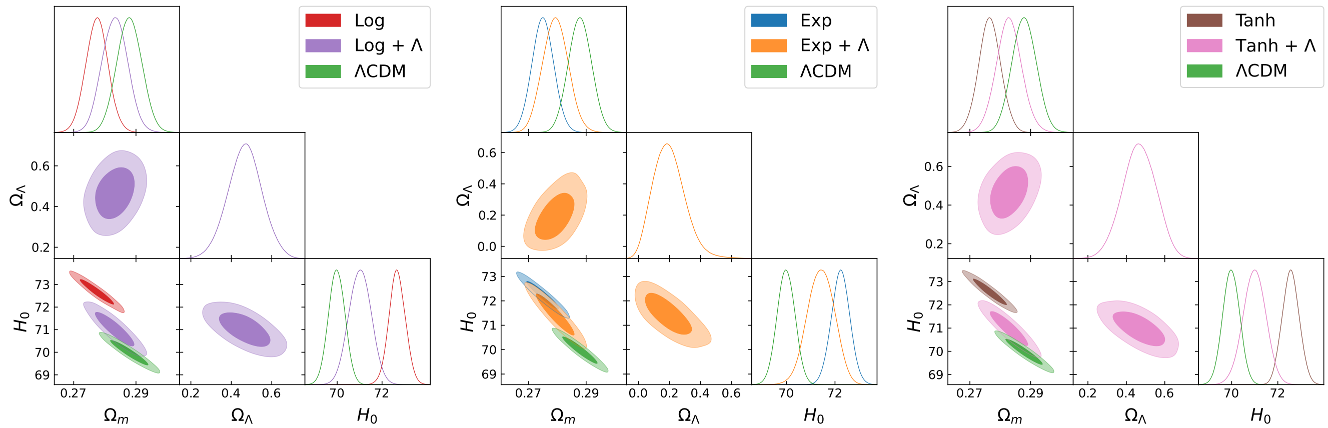

FIG. 1. 1σ and 2σ C.L. contours for the cosmological parameters $\Theta = \{\Omega_m, \Omega_\Lambda, H_0\}$. Each panel shows results for a particular $f(Q)$ gravity models, the same model assisted by the cosmological constant Λ, and ΛCDM. We show (**a**) the logarithmic form $f(Q) = Q/(8\pi G) - \alpha \ln(Q/Q_0)$, (**b**) the exponential form $f(Q) = Q/(8\pi G) \exp(\lambda Q_0/Q)$, and (**c**) the hyperbolic tangent form $f(Q) = Q/(8\pi G) + \alpha \tanh(Q_0/Q)$.

in the effective equation of state (P/ρ). There is also a singularity for Log+Λ, but it happens at a higher redshift of around $z = 6.5$. The Exp+Λ and Tanh+Λ models have a quintessence behaviour at all redshifts, in contrast to the phantom behaviour without the cosmological constant. We stress that for the $f(Q)$ models, the EoS is an *effective* EoS, meaning it does not come from a fluid but from treating the $f(Q)$ geometry as a fluid.

To obtain the dark energy EoS in the phenomenological models, we assume GR and apply the standard Friedmann equations. Figure 5 shows that these models also have a singularity. They start with phantom behaviour, with a singularity appearing around $z = 1.5$. At high redshift, the model behaves like pressureless matter instead of dark energy.

Table IV shows the statistical preference of the models relative to ΛCDM, assessed by the Bayesian evidence. ΛCDM is strongly preferred relative to the $f(Q)$ logarithmic and hyperbolic tangent models, but not any of the others. The logarithmic and hyperbolic tangent models assisted with the cosmological constant (Log + Λ and Tanh + Λ) have substantial preference on the Jeffreys scale, while the exponential and exponential assisted with the cosmological constant have strong preference. Among the more theoretically motivated $f(Q)$ models without Λ, only the Exponential model outperforms ΛCDM. Finally, the phenomenological models have very strong preference over standard ΛCDM, regardless of the assumption concerning k.

Table IV also shows that the predicted age of the Universe for all models is lower than for *Planck* 2018 flat ΛCDM ($t_0 = 13.787 \pm 0.020$ Gyr), and indeed lower than 13.6 Gyr. This is the case even for ΛCDM, which has $t_0 < 13.5$ Gyr. This is a direct consequence of the local constraints increasing H_0, since $t_0 \propto H_0^{-1}$. Thus, our work generically shows that a background solution to the Hubble and BAO tensions predicts $t_0 \lesssim 13.5$ Gyr.

In table V, we can see that only the phenomenological models have a better agreement with the DESI data than ΛCDM. The $f(Q)$ models struggle to fit the BAO data, even the exponential model. We can corroborate this in Figures 4, 6, and 7. ΛCDM struggles to fit the local H_0 determinations, as expected. The remaining models show a better fit to them, with the phenomenological models even achieving $\chi^2_{H_0} < 1$. This is due to these models predicting a higher H_0 of around 74 km/s/Mpc, whereas the $f(Q)$ models predict around 72 km/s/Mpc. The Planck fit is reasonable for all models, except for ΛCDM and the logarithmic $f(Q)$ model. ΛCDM needs a higher H_0 to reduce the tension with the local H_0 measurements, decreasing the agreement with *Planck*. Finally, all the models overfit the CC data as $\chi^2 \approx 15$, much lower than the number of CC data points (32). This suggests that the CC error bars might be overestimated. Finally, the last column shows the total χ^2. All models except for the logarithmic and hyperbolic tangent have a lower χ^2 than ΛCDM, consistent with the Bayesian evidence results. This does not necessarily mean the models are an improvement over ΛCDM, as the number of free parameters must also be considered.

VI. DISCUSSION

The first result to highlight from this paper is that it is possible to solve the Hubble tension at the background level without early-time new physics and without losing consistency with the CMB (this is in line with the recent results from [41]). We can see this from the H_0 constraints and the χ^2 results for the H_0 and Planck datasets. The only

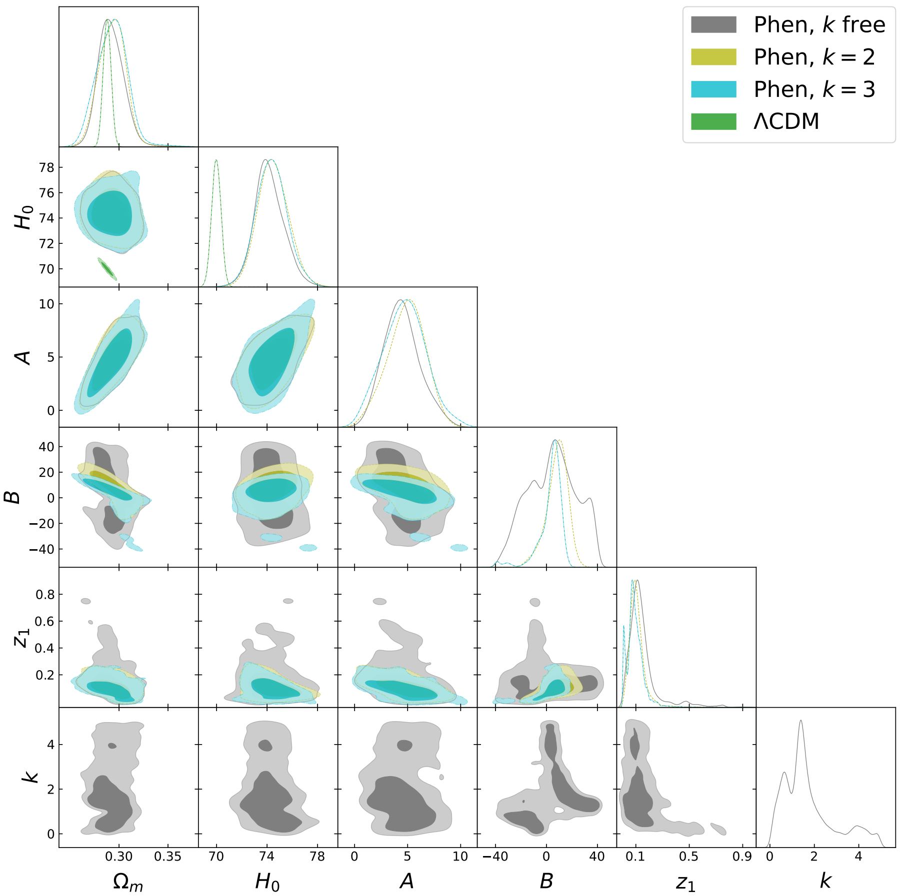

FIG. 2. 1σ and 2σ C.L. contours for the cosmological parameters $\Theta = \{\Omega_m, H_0, A, B, z_1, k\}$ in the phenomenological models where $H(z) = H_{\Lambda CDM}(z) + A\exp(-z/z_1) + B(\exp(-z/z_1) - \exp(-z/(kz_1)))$. We present the results for $k = 2$, $k = 3$, and with k as a free parameter. We also show the ΛCDM model for comparison.

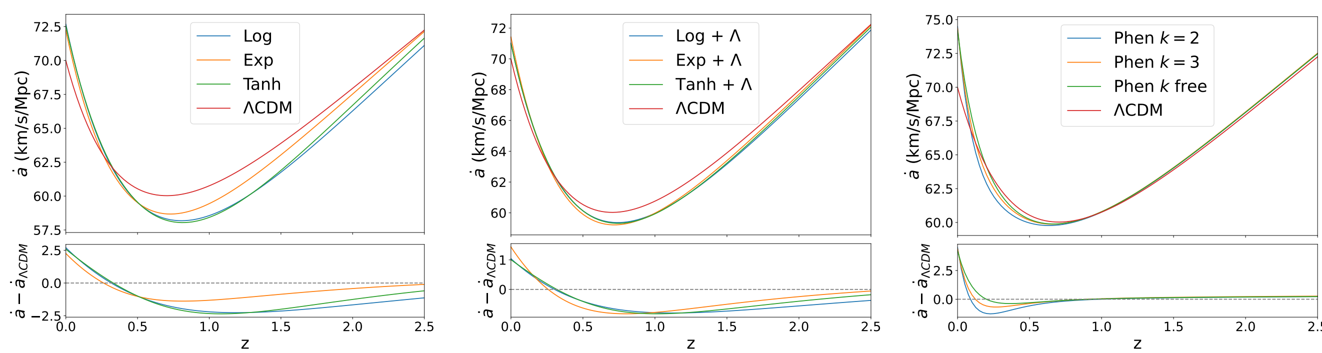

FIG. 3. Predicted $\dot{a}$ as a function of redshift for **(a)** the $f(Q)$ models, **(b)** the $f(Q)$ models assisted with the cosmological constant, and **(c)** the phenomenological models. The curves correspond to the mean values of the cosmological parameters given in tables II and III. We also plot the ΛCDM case for comparison. We include the residuals with respect to ΛCDM in the lower panels. The 1σ C.L. error bars are not visible here due to the very tight *Planck* 2018 constraints.

models that struggle to fit the *Planck* constraints are ΛCDM and the $f(Q)$ Log and Tanh models. This is interesting since ΛCDM is usually calibrated using *Planck* and is known to provide an excellent fit to the CMB *alone*, so the tension here is caused by requiring a simultaneous fit to the low-redshift H_0 measurements. By raising H_0 to try and fit the local measurements, the agreement with *Planck* is slightly worsened ($> 2\sigma$ tension). The ΛCDM model is then formally in tension with both the H_0 and *Planck* measurements.

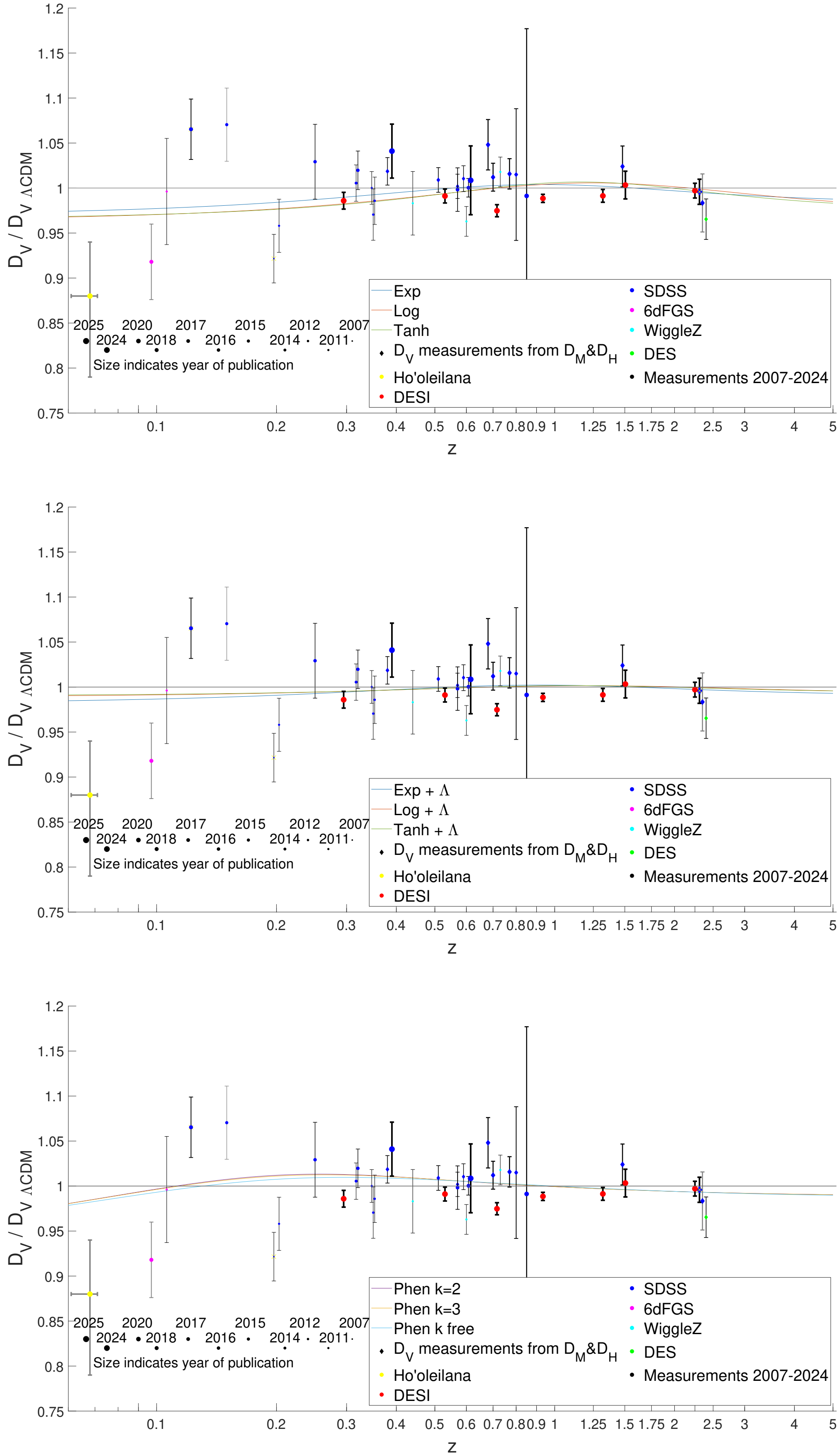

FIG. 4. Ratio between the isotropically averaged comoving BAO scale D_V to the ΛCDM case for **(a)** the $f(Q)$ models, **(b)** the $f(Q)$ models plus cosmological constant, and **(c)** the phenomenological models. We take the best fits for all models with respect to the full dataset (H_0+*Planck* 2018+CC+DESI DR2 BAO), including the ΛCDM case. We use the standard Planck sound horizon $r_d = 147.05 \pm 0.30$ Mpc. We also plot the BAO data from the last 20 years for comparison.

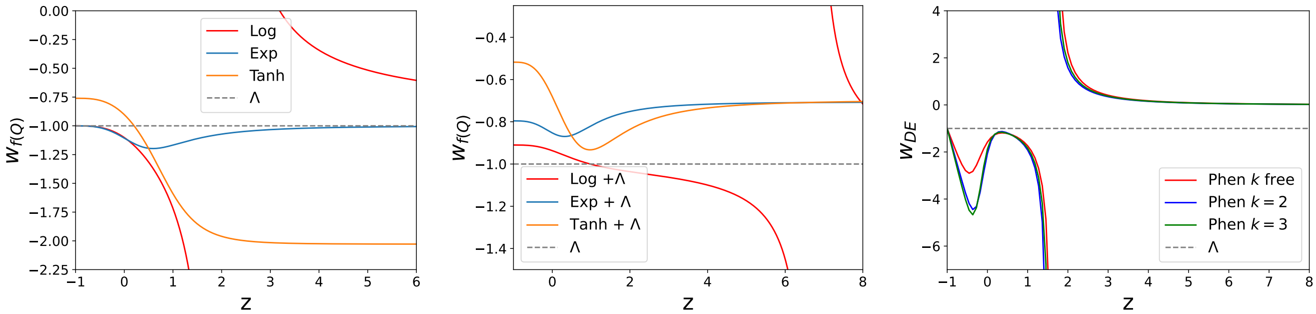

FIG. 5. Equation of state (EoS) for the effective dark energy of **(a)** the $f(Q)$ models, **(b)** the $f(Q)$ models assisted with the cosmological constant, and **(c)** the phenomenological models. The 1σ C.L. error bars are invisibly small due to the very tight *Planck* 2018 constraints.

TABLE IV. Goodness-of-fit comparison of the $f(Q)$ and phenomenological models with respect to the baseline ΛCDM model. A negative value for the log Bayes factor B means that ΛCDM is preferred, whereas a positive value means a preference for the alternative $f(Q)$ or phenomenological model. We also present the posterior predicted age of the Universe for each model.

Model	$\log B_{\text{model, }\Lambda\text{CDM}}$	Age of the Universe t_0 (Gyr)
ΛCDM	-	13.440 ± 0.027
Log	-10.288 ± 0.190	13.551 ± 0.026
Log + Λ	2.413 ± 0.195	13.478 ± 0.030
Exp	3.445 ± 0.188	13.495 ± 0.027
Exp + Λ	4.012 ± 0.192	13.474 ± 0.029
Tanh	-9.445 ± 0.190	13.536 ± 0.026
Tanh + Λ	2.123 ± 0.194	13.471 ± 0.029
Phen $k = 2$	8.395 ± 0.205	13.458 ± 0.110
Phen $k = 3$	8.010 ± 0.207	13.458 ± 0.124
Phen k free	8.543 ± 0.203	13.450 ± 0.108

The next important result is that the $f(Q)$ models perform worse than ΛCDM with the DESI DR2 data. Their χ^2 values are considerably higher than the number of data points, which indicates a tension with the data. We can also see a trend for the $f(Q)$ models when adding the cosmological constant Λ, which significantly reduces χ^2_{DESI} to nearly the ΛCDM value. This reduces the overall χ^2, despite the larger $\chi^2_{H_0}$ contribution. We can visually see the BAO tensions of these models in figures 4, 6, and 7.

The phenomenological models outperform ΛCDM in their fit to the BAO data, with $\chi^2_{\text{DESI}} \approx 10$ (in comparison to ΛCDM $\chi^2_{\text{DESI}} = 15.14$). They are in general the best models. However, they have five (or six) parameters, in contrast to two (or three) for ΛCDM and the $f(Q)$ models. Furthermore, they are not theoretically motivated, unlike the $f(Q)$ models. On the other hand, Figures 4, 6, and 7 illustrate their good agreement with the great majority of BAO data accumulated over the last 20 years. Table IV also shows that these models have a Bayesian evidence considerably

TABLE V. Minimum χ^2 contributions for the considered models. We report the contributions for the different observational constraints (DESI DR2 BAO, local H0, *Planck* 2018, Cosmic Chronometers). We also show the number of data points in each catalogue.

Data Points	13	4	2	32	51
Model	χ^2_{DESI}	$\chi^2_{H_0}$	χ^2_{Planck}	χ^2_{CC}	χ^2_{total}
ΛCDM	15.14	15.39	5.81	15.40	51.73
Log	35.95	6.04	7.67	16.38	66.05
Log + Λ	18.88	9.21	1.28	15.35	44.71
Exp	25.33	4.63	0.16	15.36	45.47
Exp + Λ	19.50	6.77	1.15	15.18	42.60
Tanh	38.35	6.34	3.95	16.47	65.12
Tanh + Λ	18.62	9.48	1.98	15.36	45.44
Phen $k = 2$	10.15	0.47	1.56	14.92	27.11
Phen $k = 3$	10.43	0.52	1.54	14.86	27.37
Phen k free	10.96	0.52	1.22	14.83	27.53

higher than ΛCDM, so that empirically speaking, they afford a compelling solution to the Hubble and BAO tensions. Another highlight for these models is that the mean values for z_1 are quite small ($z_1 \leq 0.15$). This suggests that to solve the Hubble tension consistently with BAO data, we need an extra acceleration term beyond ΛCDM that only arises at very low redshift [in the $z < 0.15$ regime of 42], hinting that the solution to both problems lies within the third rung of the distance ladder. Importantly, the inferred $z_1 \ll z_\Lambda$, where $z_\Lambda \approx 0.5$ is the redshift at which $\ddot{a}$ switches sign due to dark energy or something with a similar effect. If the observed accelerated expansion of the Universe is not due to Λ but instead arises from some other cause like a geometric effect, we would expect our phenomenological model to indicate that departures from ΛCDM set in when Λ becomes dominant, i.e., that $z_1 \approx z_\Lambda$. This is not the case, indicating that the deviation from ΛCDM identified by the phenomenological model and necessary to solve the Hubble and BAO tensions is probably not related to alternative interpretations of the accelerated cosmic expansion.

While a departure from the ΛCDM expansion history at such low z is possible, the low inferred z_1 in the phenomenological models might instead be interpreted to mean that the solution is local in nature. This is possible if we live in a large local underdensity or void, as suggested by galaxy number counts [102]. A model set up along those lines to solve the Hubble tension [103] correctly predicted the BAO anomaly [13]. The main difference is that this solution involves modifications to ΛCDM at the perturbation level with a background *Planck* cosmology, in contrast to the purely background phenomenological solutions that retain the assumption of purely cosmological redshift.

The Bayesian evidence shows that the Log and Tanh $f(Q)$ models provide a fit much worse than standard ΛCDM, so they cannot be considered candidates to solve the Hubble tension while achieving BAO consistency. Yet when adding the cosmological constant, these models out-perform ΛCDM, with substantial evidence. This comes at the cost of undermining their theoretical motivation, which was to explain the accelerated expansion of the Universe without dark energy [33, 34]. Adding the cosmological constant reduces the effective geometric density to $\Omega_\alpha = 0.249 \pm 0.085$ for Log and $\Omega_\alpha = 0.254 \pm 0.088$ for Tanh. Thus, the modified models can only explain around a third of the dark energy.

On the other hand, the exponential $f(Q)$ model has strong preference against the flat ΛCDM model using the Jeffreys scale. It is interesting that this is the case without the assistance of the cosmological constant. This puts the model in a good position to solve the Hubble tension. Nevertheless, as we can see in table V, it is not fully consistent with BAO. The $\chi^2_{\rm DESI}$ contribution is more than 10 units higher than ΛCDM, which has the same number of parameters. This highlights the difficulties with solving the Hubble tension and being consistent with BAO data at the same time. The exponential model assisted with the cosmological constant has better agreement with BAO, although still not as good as ΛCDM, and thus not fully consistent with DESI DR2 BAO. In this case, the evidence is higher (with a Bayes factor > 4). Interestingly, $\Omega_m + \Omega_\Lambda = 0.475 \pm 0.105$, so geometry accounts for more than 50% of the effective content of the Universe. From the above, we conclude that the considered $f(Q)$ models cannot fully solve the Hubble tension while producing BAO consistency, even if they are assisted by the cosmological constant (+Λ).

In table IV, we can see the effect that raising H_0 has on the models. The age of the universe is given by

$$t_0 = \frac{1}{H_0} \int_0^\infty dz \, \frac{a}{E(z)} \tag{42}$$

where $E(a) \equiv H(a)/H_0$ is the reduced Hubble factor. The comoving distance to recombination is given by a similar integral, but with c in the numerator instead of a (Eq. 38). To achieve the *Planck* distance to recombination and be consistent with local H_0, we need to decrease $1/H(z)$ at low redshift and compensate by exceeding ΛCDM at high redshift to produce the same integral. However, the age of the Universe integral has an extra factor of a in the numerator, making changes at low z relatively more important. This means that decreasing $1/H(z)$ at low z has a bigger impact, since $a \approx 1$ in this range. At high redshift, increasing $1/H(z)$ has the opposite effect, but high redshifts play a smaller role because these are downweighted by the small a. This means that raising H_0 to match the local measurements while preserving the comoving distance to recombination has an overall effect of reducing the age of the universe. This means all the models predict lower ages for the universe. These ages are in the range $13.45 - 13.55$ Gyr with small uncertainties, since we use tight *Planck* constraints [4]. The extent to which these ages are possible can be quantified using the ages of the oldest stars [17] and globular clusters [18]. There are stars with ages higher than 13.3 Gyr [17], so the Universe must be older than this age. The samples considered in their study have an inverse variance weighted mean age of 14.05 ± 0.25 Gyr, implying that $t_0 \approx 14.25 \pm 0.25$ Gyr if the objects they studied took 200 Myr to form. The models considered in this paper are therefore in $\approx 3\sigma$ tension with their estimated age of the Universe. Indeed, those authors found that $H_0 < 73$ km/s/Mpc (assuming ΛCDM) with a probability of 90.3% [17]. Furthermore, globular clusters imply the age of the Universe is $t_0 = 13.57^{+0.16}_{-0.14}\,(\text{stat}) \pm 0.23\,(\text{sys})$ Gyr [18]. Since those authors report that the oldest globular cluster has an age of 13.39 Gyr, this implicitly assumes a formation time of only 180 Myr. Assuming this is valid, all the considered models studied in this paper lie within the 1σ C.L. of the age reported by [18]. Future studies will shed more light on whether lower ages of the Universe than ΛCDM *Planck* are feasible, a necessary feature for background late-time solutions to the Hubble tension. This is also a feature of models that solve only the BAO anomaly without considering the Hubble tension, since the BAO anomaly implies a smaller comoving distance to $z \approx 1$ than *Planck* ΛCDM [13]. For instance, the CPL $w_0 w_a$ parametrization implies an age of $t_0 = 13.56$ Gyr (using DESI DR2+CMB data), in line with the models considered in this paper.

Figure 5 highlights several problems that some of the models have. The Log and Log+Λ models have a singularity in the effective dark energy EoS. This comes from the effective density changing from positive to negative, while the effective pressure was negative. But since this is an effective EoS, there is no singularity in the true EoS because the universe in this cosmology is composed only of matter and radiation. For the phenomenological models, this is not the case as it is a true EoS coming from dark energy. The singularity in them is a true pathology for the models. Therefore, despite the observational successes (alleviating the Hubble and BAO tensions simultaneously), the phenomenological models imply an unphysical energy density, violating the weak energy condition. While this suggests the model is not physically viable as a simple dark energy fluid in General Relativity, it might instead point towards new physics in the form of modified theories of gravity. They might accommodate a solution like (29) which can solve the observational tensions studied in this paper. The remaining models do not have singularity problems. The Exp model shows a phantom behaviour converging to the cosmological constant at high redshift and also at $z = -1$, which represents the infinite future. This is crucial as phantom behaviour when $z \to -1$ implies a Big Rip. The Exp + Λ model has a quintessence behaviour at all times, showing that the cosmological constant increases the EoS and decreases the accelerated expansion, leading to a lower H_0. We see the same behaviour with the Tanh model when adding the cosmological constant. This changes a phantom crossing model to a purely quintessence model.

VII. CONCLUSIONS

We study modifications to the ΛCDM background evolution in the context of the Hubble and BAO tensions. We focus on three $f(Q)$ modified gravity models and three phenomenological models that modify the ΛCDM $H(z)$ with a double exponential behaviour (29). The theoretical models are given by $f(Q) = Q/(8\pi G) - \alpha \ln(Q/Q_0)$ ("Log"), $f(Q) = Q/(8\pi G)\exp(\lambda Q_0/Q)$ ("Exp"), and $f(Q) = Q/(8\pi G) + \alpha \tanh(Q_0/Q)$ ("Tanh"). We also consider the same models assisted with the cosmological constant ("$+\Lambda''$).

We constrained the cosmological parameters with four different datasets: local H_0 measurements, DESI DR2 BAO data, *Planck* 2018 constraints on the comoving distance to recombination and $\Omega_m h^2$, and CC. We used a nested sampling algorithm to sample the posterior probability and compute the Bayesian evidence. The $f(Q)$ and phenomenological models are capable of solving the Hubble tension, having best-fit $H_0 \approx 72$ km/s/Mpc and 74 km/s/Mpc, respectively. The $f(Q)$ models assisted with the cosmological constant have $H_0 \approx 71$ km/s/Mpc, alleviating but not completely solving the Hubble tension. However, the $f(Q)$ models cannot fit the 13 DESI DR2 BAO data points [12] very well. They have $\chi^2_{\rm BAO,min} > 25$ for the Exp model and $\chi^2_{\rm BAO,min} > 35$ for the Log and Tanh models, considerably higher than the number of data points (13) and the ΛCDM result ($\chi^2_{\rm BAO,\Lambda CDM} = 15.14$). The $f(Q)$ models assisted with the cosmological constant perform better with $\chi^2_{\rm BAO,min} \approx 18 - 19$, although this is still higher than for ΛCDM. The phenomenological models have $\chi^2_{\rm BAO,min} \approx 10$ and are therefore able to solve the Hubble tension while retaining BAO consistency.

The Log and Tanh models have a Bayesian evidence much lower than ΛCDM, with $\log B \approx -10$. The remaining models have more evidence than ΛCDM. Interestingly, the Exp model has $\log B \approx 3$, showing strong preference in the Jeffreys scale over ΛCDM without the assistance of the cosmological constant, which only slightly helps. The phenomenological models have $\log B \approx 8$ and therefore work very well. All the models predict an age of the Universe of $t_0 \approx 13.45 - 13.55$ Gyr, well below the Planck ΛCDM age of 13.80 Gyr due to the high local H_0 measurements and the low observed comoving distance to $z \lesssim 1$ from DESI DR2 BAO [12].

The Exp model is capable of providing a reasonable solution to the cosmological tensions studied in this paper. It alleviates the Hubble tension, but it struggles to fit the BAO data. The model is nonetheless preferred over ΛCDM using the Bayesian evidence. Furthermore, it is theoretically motivated as a dark energy candidate, in contrast to the models assisted with the cosmological constant Λ and the phenomenological models. The $f(Q)$ models with Λ have a higher Bayesian evidence, showing that they fit the data better, even if their theoretical motivation is undermined. The phenomenological models offer a compelling *empirical* solution to the tensions, but are not theoretically motivated and predict a singularity in their dark energy EoS. This comes from the fluid energy density becoming negative and thus breaking the weak energy condition, implying that these models are unphysical in GR – though they could potentially be valid solutions of another theory. The phenomenological models behave like ΛCDM across most of the relevant redshift range, with an extra expansion term at $z \leq 0.15$ to match the low-redshift data. This suggests that the solution to the Hubble and BAO tensions lies at low redshift, perhaps even within the range of the distance ladder.

ACKNOWLEDGEMENTS

HD, JAN, and IB are supported by Royal Society University Research Fellowship 211046.

VIII. DATA AVAILABILITY

No new data is produced in this work. We will make our code publicly available on publication of the paper.

Appendix A: Comparison of best-fitting models to BAO measurements over the last 20 years

In our main analysis, we constrain our models using BAO measurements only from DESI DR2 [12]. These are not the only BAO measurements. We therefore compare the best-fitting model in each case to all available BAO measurements over the last 20 years [table 1 of 13, and references therein]. Figure 6 shows our results for D_H, while Figure 7 shows D_M instead.

---

[1] A. Einstein. Die Feldgleichungen der Gravitation. *Sitzungsberichte der Königlich Preußischen Akademie der Wissenschaften (Berlin)*, 6:844–847, 1915.
[2] G. Efstathiou, W. J. Sutherland and S. J. Maddox. The cosmological constant and cold dark matter. *Nature*, 348(6303):705–707, dec 1990.
[3] J. P. Ostriker and P. J. Steinhardt. The observational case for a low-density Universe with a non-zero cosmological constant. *Nature*, 377:600–602, oct 1995.
[4] Planck Collaboration VI. Planck 2018 results. VI. Cosmological parameters. *A&A*, 641:A6, sep 2020.
[5] E. Calabrese et al. The Atacama Cosmology Telescope: DR6 Constraints on Extended Cosmological Models. *JCAP*, in press, mar 2025.
[6] E. Camphuis et al. SPT-3G D1: CMB temperature and polarization power spectra and cosmology from 2019 and 2020 observations of the SPT-3G Main field. *ArXiv e-prints*, Arxiv, jun 2025.
[7] S. Mazurenko, I. Banik and P. Kroupa. The redshift dependence of the inferred H_0 in a local void solution to the Hubble tension. *MNRAS*, 536(4):3232–3241, feb 2025.
[8] E. Di Valentino et al. The CosmoVerse White Paper: Addressing observational tensions in cosmology with systematics and fundamental physics. *Physics of the Dark Universe*, 49:101965, sep 2025.
[9] D. J. Eisenstein and W. Hu. Baryonic Features in the Matter Transfer Function. *ApJ*, 496(2):605–614, mar 1998.
[10] S. Cole et al. The 2dF Galaxy Redshift Survey: power-spectrum analysis of the final data set and cosmological implications. *MNRAS*, 362(2):505–534, sep 2005.
[11] D. J. Eisenstein et al. Detection of the Baryon Acoustic Peak in the Large-Scale Correlation Function of SDSS Luminous Red Galaxies. *ApJ*, 633(2):560–574, nov 2005.
[12] DESI Collaboration. DESI DR2 results. II. Measurements of baryon acoustic oscillations and cosmological constraints. *Physical Review D*, 112(8):083515, oct 2025.
[13] I. Banik and V. Kalaitzidis. Testing the local void hypothesis using baryon acoustic oscillation measurements over the last 20 yr. *MNRAS*, 540(1):545–561, jun 2025.
[14] R. H. Cyburt et al. Big bang nucleosynthesis: Present status. *Reviews of Modern Physics*, 88:015004, feb 2016.
[15] S. Hamidreza Mirpoorian, K. Jedamzik and L. Pogosian. Is Dynamical Dark Energy Necessary? DESI BAO and Modified Recombination. *ArXiv e-prints*, Arxiv, apr 2025.
[16] S. Vagnozzi. Seven Hints That Early-Time New Physics Alone Is Not Sufficient to Solve the Hubble Tension. *Universe*, 9(9):393, aug 2023.
[17] A. Cimatti and M. Moresco. Revisiting oldest stars as cosmological probes. *ApJ*, 953(2):149, aug 2023.
[18] D. Valcin et al. The Age of the Universe with Globular Clusters III: Gaia distances and hierarchical modeling. *ArXiv e-prints*, Arxiv, mar 2025.
[19] I. Banik and N. Samaras. Constraints on the Hubble and matter density parameters with and without modelling the CMB anisotropies. *ArXiv e-prints*, Arxiv, oct 2025.
[20] J. M. Nester and H.-J. Yo. Symmetric teleparallel general relativity. *arXiv preprint gr-qc/9809049*, 1998.
[21] J. Beltran Jimenez, L. Heisenberg and T. S. Koivisto. The geometrical trinity of gravity. *Universe*, 5(7):173, 2019.
[22] A. De Felice and S. Tsujikawa. f (r) theories. *Living Reviews in Relativity*, 13(1):1–161, 2010.
[23] J. B. Jiménez, L. Heisenberg and T. Koivisto. Coincident general relativity. *Physical Review D*, 98(4):044048, aug 2018.
[24] J. B. Jiménez et al. Cosmology in f (Q) geometry. *Physical Review D*, 101(10):103507, may 2020.
[25] B. J. Barros et al. Testing f (q) gravity with redshift space distortions. *Physics of the Dark Universe*, 30:100616, 2020.
[26] S. Mandal, D. Wang and P. Sahoo. Cosmography in f (q) gravity. *Physical Review D*, 102(12):124029, 2020.

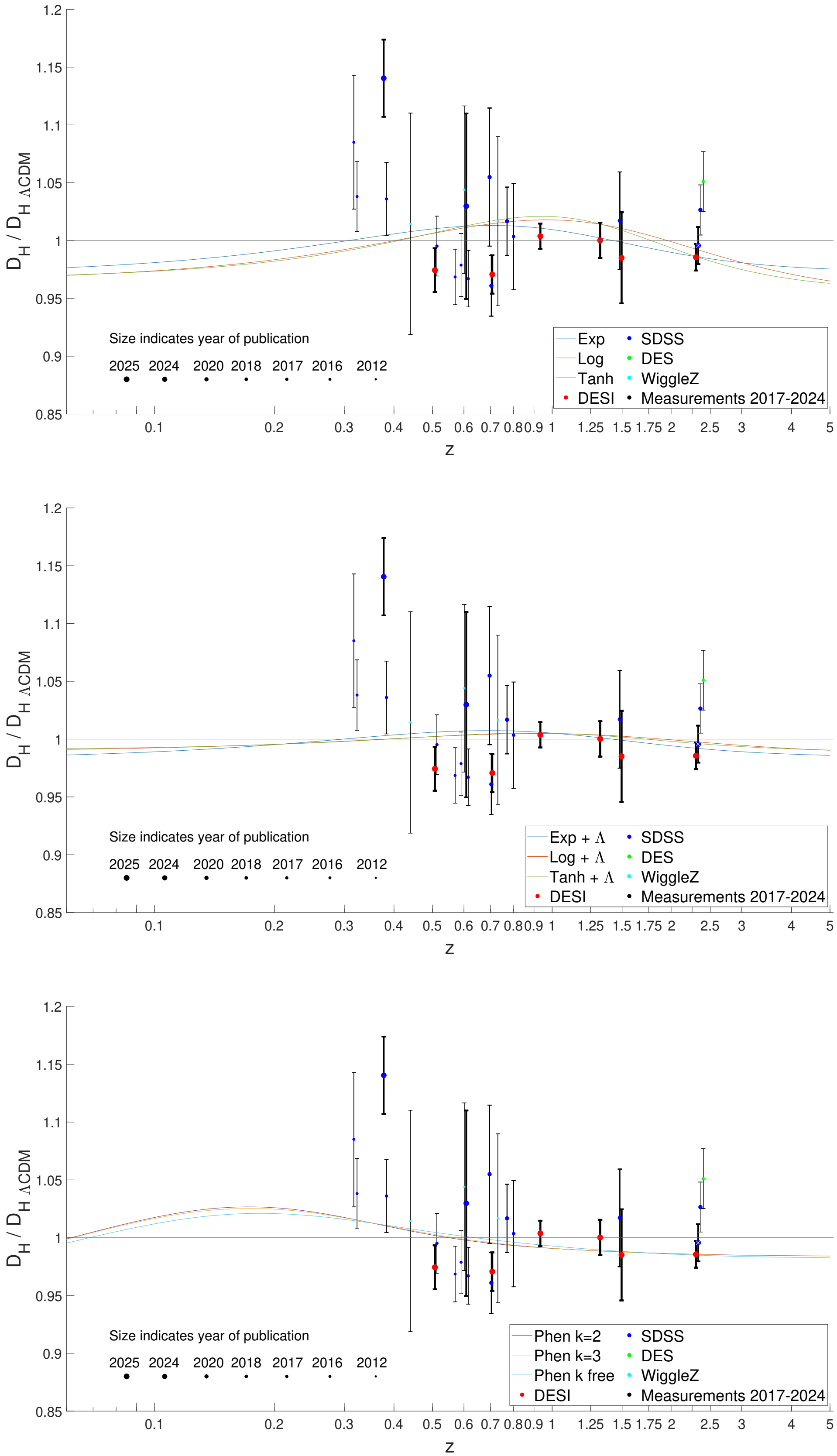

FIG. 6. Ratio between the Hubble distance D_H and the ΛCDM case. We take the best fits for all models with respect to the full data set (H_0+*Planck* 2018+CC+DESI DR2 BAO), including the ΛCDM case. We consider the standard Planck sound horizon $r_d = 147.05 \pm 0.30$ Mpc. We also plot the BAO data from the last 20 years for comparison. We present the results for **(a)** the $f(Q)$ models, **(b)** the $f(Q)$ models assisted with the cosmological constant, and **(c)** the phenomenological models.

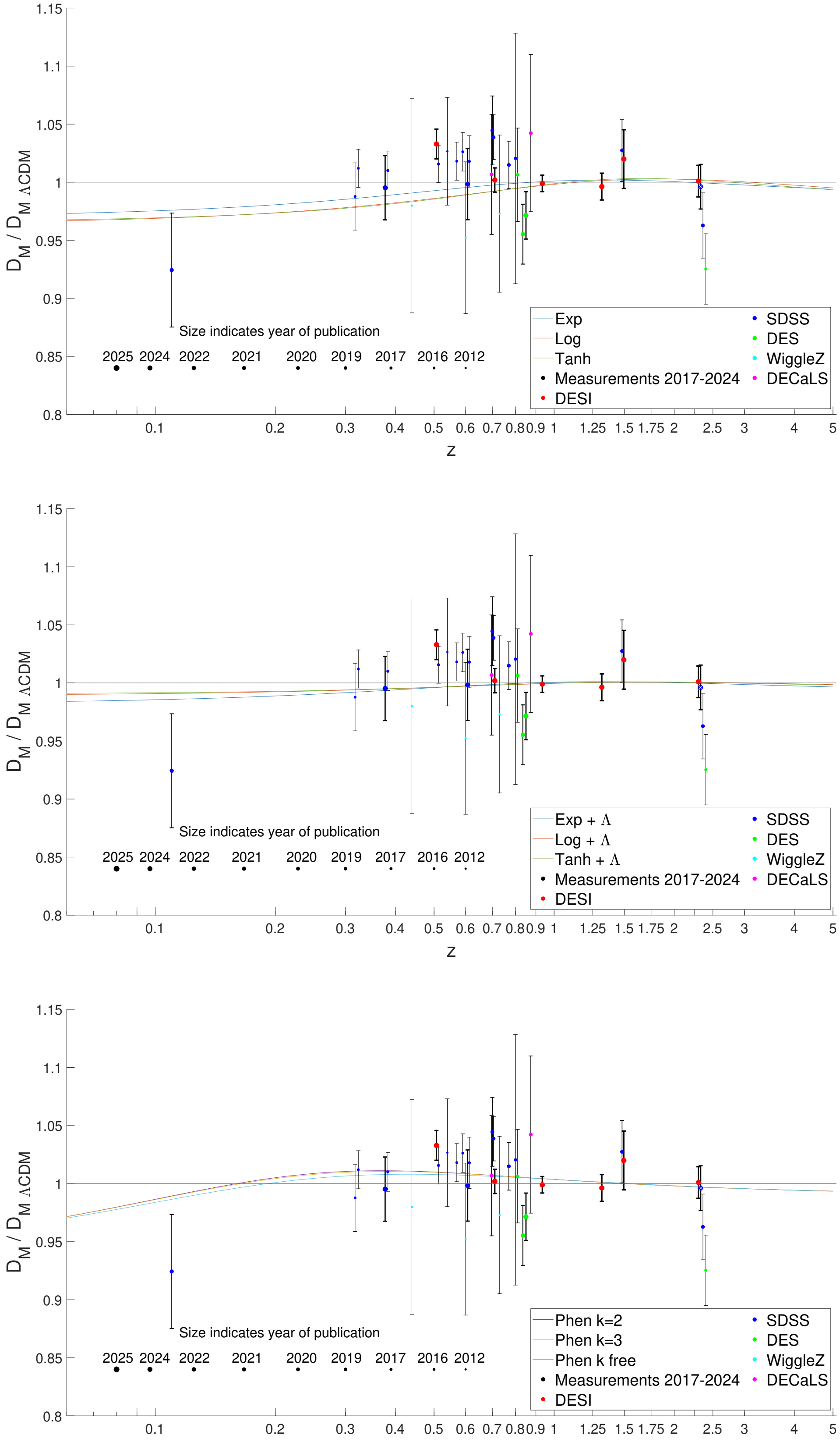

FIG. 7. Ratio between the comoving distance D_M and the ΛCDM case. We take the best fits for all models with respect to the full data set (H_0+*Planck* 2018+CC+DESI DR2 BAO), including the ΛCDM case. We consider the standard Planck sound horizon $r_d = 147.05 \pm 0.30$ Mpc. We also plot the BAO data from the last 20 years for comparison. We present the results for **(a)** the $f(Q)$ models, **(b)** the $f(Q)$ models assisted with the cosmological constant, and **(c)** the phenomenological models.

[27] S. Mandal, P. Sahoo and J. R. Santos. Energy conditions in f (q) gravity. *Physical Review D*, 102(2):024057, 2020.

[28] N. Dimakis, A. Paliathanasis and T. Christodoulakis. Quantum cosmology in f (q) theory. *Classical and Quantum Gravity*, 38(22):225003, 2021.

[29] F. D'Ambrosio, L. Heisenberg and S. Kuhn. Revisiting cosmologies in teleparallelism. *Classical and Quantum Gravity*, 39(2):025013, jan 2022.

[30] M. Hohmann. General covariant symmetric teleparallel cosmology. *Physical Review D*, 104(12):124077, dec 2021.

[31] S. Mandal et al. Cosmological observational constraints on the power law f (q) type modified gravity theory. *The European Physical Journal C*, 83(12):1141, 2023.

[32] F. K. Anagnostopoulos, S. Basilakos and E. N. Saridakis. First evidence that non-metricity f(Q) gravity could challenge ΛCDM. *Physics Letters B*, 822:136634, nov 2021.

[33] J. A. Nájera, C. Aráoz Alvarado and C. Escamilla-Rivera. Constraints on f (Q) logarithmic model using gravitational wave standard sirens. *MNRAS*, 524(4):5280–5290, oct 2023.

[34] F. K. Anagnostopoulos et al. New models and big bang nucleosynthesis constraints in f(Q) gravity. *European Physical Journal C*, 83(1):58, jan 2023.

[35] R. D'Agostino and R. C. Nunes. Forecasting constraints on deviations from general relativity in f (q) gravity with standard sirens. *Physical Review D*, 106(12):124053, 2022.

[36] S. Capozziello and M. Capriolo. Gravitational waves in f (q) non-metric gravity without gauge fixing. *Physics of the Dark Universe*, 45:101548, 2024.

[37] S. Capozziello, M. Capriolo and S. Nojiri. Gravitational waves in f (q) non-metric gravity via geodesic deviation. *Physics Letters B*, 850:138510, 2024.

[38] W. Wang, K. Hu and T. Katsuragawa. Solar System tests in covariant f(Q) gravity. *Phys. Rev. D*, 111(6):064038, 2025.

[39] Z. Sakr and L. Schey. Investigating the Hubble tension and σ_8 discrepancy in f(Q) cosmology. *JCAP*, 10:052, 2024.

[40] C. G. Boiza et al. Addressing H_0 and S_8 tensions within $f(Q)$ cosmology. *ArXiv e-prints*, Arxiv, may 2025.

[41] N. S. Kavya, S. Swagat Mishra and P. K. Sahoo. f(q) gravity as a possible resolution of the h0 and s8 tensions with desi dr2. *Scientific Reports*, 15:36504, 10 2025.

[42] A. G. Riess et al. A Comprehensive Measurement of the Local Value of the Hubble Constant with 1 km s^{-1} Mpc^{-1} Uncertainty from the Hubble Space Telescope and the SH0ES Team. *ApJL*, 934(1):L7, jul 2022.

[43] E. Snapper and R. J. Troyer. *Metric affine geometry*. Elsevier, 2014.

[44] S. Bahamonde et al. Teleparallel gravity: from theory to cosmology. *Reports on Progress in Physics*, 86(2):026901, 2023.

[45] L. Heisenberg. Review on f (q) gravity. *Physics Reports*, 1066:1–78, 2024.

[46] J. W. Maluf. The teleparallel equivalent of general relativity. *Annalen der Physik*, 525(5):339–357, 2013.

[47] Y.-F. Cai et al. f (t) teleparallel gravity and cosmology. *Reports on Progress in Physics*, 79(10):106901, 2016.

[48] J. Shi. Cosmological constraints in covariant f(Q) gravity with different connections. *European Physical Journal C*, 83(10):951, oct 2023.

[49] S. A. Narawade, S. V. Lohakare and B. Mishra. Stable $f(Q)$ gravity model through non-trivial connection. *Annals of Physics*, 474:169913, mar 2025.

[50] I. Ayuso et al. Insights in $f(Q)$ cosmology: the relevance of the connection. *JCAP*, in press, jun 2025.

[51] M. Chevallier and D. Polarski. Accelerating Universes with Scaling Dark Matter. *International Journal of Modern Physics D*, 10(2):213–223, jan 2001.

[52] E. V. Linder. Exploring the Expansion History of the Universe. *Physical Review Letters*, 90(9):091301, mar 2003.

[53] E. V. Linder. The dynamics of quintessence, the quintessence of dynamics. *General Relativity and Gravitation*, 40(2-3):329–356, feb 2008.

[54] L. Breuval et al. Small Magellanic Cloud Cepheids Observed with the Hubble Space Telescope Provide a New Anchor for the SH0ES Distance Ladder. *ApJ*, 973(1):30, sep 2024.

[55] M. Visser and C. Barcelo. Energy conditions and their cosmological implications. In *3rd International Conference on Particle Physics and the Early Universe*, pp. 98–112. World Scientific, 2000.

[56] M. Moresco et al. Unveiling the Universe with emerging cosmological probes. *Living Reviews in Relativity*, 25(1):6, dec 2022.

[57] D. W. Pesce et al. The Megamaser Cosmology Project. XIII. Combined Hubble Constant Constraints. *ApJ*, 891(1):L1, mar 2020.

[58] J. B. Jensen et al. The TRGB-SBF Project. III. Refining the HST Surface Brightness Fluctuation Distance Scale Calibration with JWST. *ApJ*, 987(1):87, jul 2025.

[59] C. Vogl et al. No rungs attached: A distance-ladder free determination of the Hubble constant through type II supernova spectral modelling. *Astron. Astrophys.*, 702:A41, 2025.

[60] M. Moresco et al. Setting the Stage for Cosmic Chronometers. II. Impact of Stellar Population Synthesis Models Systematics and Full Covariance Matrix. *ApJ*, 898(1):82, jul 2020.

[61] H. S. Leavitt and E. C. Pickering. Periods of 25 Variable Stars in the Small Magellanic Cloud. *Harvard College Observatory Circular*, 173:1–3, mar 1912.

[62] R. Jimenez and A. Loeb. Constraining Cosmological Parameters Based on Relative Galaxy Ages. *ApJ*, 573(1):37–42, jul 2002.

[63] `https://dynesty.readthedocs.io/en/v2.1.5/`.

[64] J. S. Speagle. DYNESTY: a dynamic nested sampling package for estimating Bayesian posteriors and evidences. *MNRAS*, 493(3):3132–3158, apr 2020.

[65] S. Koposov et al. joshspeagle/dynesty: v2.1.4. *Zenodo*, jun 2024.

[66] J. Skilling. Nested Sampling. In R. Fischer, R. Preuss and U. V. Toussaint, editors, *Bayesian Inference and Maximum Entropy Methods in Science and Engineering: 24th International Workshop on Bayesian Inference and Maximum Entropy Methods in Science and Engineering*, volume 735 of *American Institute of Physics Conference Series*, pp. 395–405. AIP, nov 2004.
[67] J. Skilling. Nested sampling for general Bayesian computation. *Bayesian Analysis*, 1(4):833–859, 2006.
[68] F. Feroz, M. P. Hobson and M. Bridges. MULTINEST: an efficient and robust Bayesian inference tool for cosmology and particle physics. *MNRAS*, 398(4):1601–1614, oct 2009.
[69] `https://getdist.readthedocs.io/en/latest/`.
[70] A. Lewis. GetDist: a Python package for analysing Monte Carlo samples. *JCAP*, 2025(8):025, aug 2025.
[71] R. E. Kass and A. E. Raftery. Bayes factors. *Journal of the American Statistical Association*, 90(430):773–795, 1995.
[72] R. Trotta. Bayes in the sky: Bayesian inference and model selection in cosmology. *Contemporary Physics*, 49(2):71–104, mar 2008.
[73] R. B. Tully, C. Howlett and D. Pomarède. Ho'oleilana: An Individual Baryon Acoustic Oscillation? *ApJ*, 954(2):169, sep 2023.
[74] E. de Carvalho et al. BAO angular scale at $z_{eff} = 0.11$ with the SDSS blue galaxies. *A&A*, 649:A20, may 2021.
[75] P. Carter et al. Low redshift baryon acoustic oscillation measurement from the reconstructed 6-degree field galaxy survey. *MNRAS*, 481(2):2371–2383, dec 2018.
[76] A. J. Ross et al. The clustering of the SDSS DR7 main Galaxy sample - I. A 4 per cent distance measure at z = 0.15. *MNRAS*, 449(1):835–847, may 2015.
[77] W. J. Percival et al. Measuring the Baryon Acoustic Oscillation scale using the Sloan Digital Sky Survey and 2dF Galaxy Redshift Survey. *MNRAS*, 381(3):1053–1066, nov 2007.
[78] W. J. Percival et al. Baryon acoustic oscillations in the Sloan Digital Sky Survey Data Release 7 galaxy sample. *MNRAS*, 401(4):2148–2168, feb 2010.
[79] C.-H. Chuang et al. The clustering of galaxies in the completed SDSS-III Baryon Oscillation Spectroscopic Survey: single-probe measurements from DR12 galaxy clustering - towards an accurate model. *MNRAS*, 471(2):2370–2390, oct 2017.
[80] L. Anderson et al. The clustering of galaxies in the SDSS-III Baryon Oscillation Spectroscopic Survey: baryon acoustic oscillations in the Data Releases 10 and 11 Galaxy samples. *MNRAS*, 441(1):24–62, jun 2014.
[81] S. Alam et al. The clustering of galaxies in the completed SDSS-III Baryon Oscillation Spectroscopic Survey: cosmological analysis of the DR12 galaxy sample. *MNRAS*, 470(3):2617–2652, sep 2017.
[82] C.-H. Chuang, Y. Wang and M. D. P. Hemantha. A robust distance measurement and dark energy constraints from the spherically averaged correlation function of Sloan Digital Sky Survey luminous red Galaxies. *MNRAS*, 423(2):1474–1484, jun 2012.
[83] C.-H. Chuang and Y. Wang. Measurements of H(z) and D_A(z) from the two-dimensional two-point correlation function of Sloan Digital Sky Survey luminous red galaxies. *MNRAS*, 426(1):226–236, oct 2012.
[84] M. M. Ivanov, M. Simonović and M. Zaldarriaga. Cosmological parameters from the BOSS galaxy power spectrum. *JCAP*, 2020(5):042, may 2020.
[85] A. P. Schirra, M. Quartin and L. Amendola. A model-independent measurement of the expansion and growth rates from BOSS using the FreePower method. *Physics of the Dark Universe*, 49:102033, sep 2025.
[86] H.-J. Seo et al. Acoustic Scale from the Angular Power Spectra of SDSS-III DR8 Photometric Luminous Galaxies. *ApJ*, 761(1):13, dec 2012.
[87] Z. Slepian et al. Detection of baryon acoustic oscillation features in the large-scale three-point correlation function of SDSS BOSS DR12 CMASS galaxies. *MNRAS*, 469(2):1738–1751, aug 2017.
[88] H. Gil-Marín et al. The Completed SDSS-IV extended Baryon Oscillation Spectroscopic Survey: measurement of the BAO and growth rate of structure of the luminous red galaxy sample from the anisotropic power spectrum between redshifts 0.6 and 1.0. *MNRAS*, 498(2):2492–2531, oct 2020.
[89] G.-B. Zhao et al. The completed SDSS-IV extended Baryon Oscillation Spectroscopic Survey: a multitracer analysis in Fourier space for measuring the cosmic structure growth and expansion rate. *MNRAS*, 504(1):33–52, jun 2021.
[90] Y. Wang et al. The clustering of the SDSS-IV extended baryon oscillation spectroscopic survey DR16 luminous red galaxy and emission-line galaxy samples: cosmic distance and structure growth measurements using multiple tracers in configuration space. *MNRAS*, 498(3):3470–3483, nov 2020.
[91] F. Zhu et al. The clustering of theSDSS-IV extended Baryon Oscillation Spectroscopic Survey DR14 quasar sample: measuring the anisotropic baryon acoustic oscillations with redshift weights. *MNRAS*, 480(1):1096–1105, oct 2018.
[92] A. de Mattia et al. The completed SDSS-IV extended Baryon Oscillation Spectroscopic Survey: measurement of the BAO and growth rate of structure of the emission line galaxy sample from the anisotropic power spectrum between redshift 0.6 and 1.1. *MNRAS*, 501(4):5616–5645, mar 2021.
[93] R. Neveux et al. The completed SDSS-IV extended Baryon Oscillation Spectroscopic Survey: BAO and RSD measurements from the anisotropic power spectrum of the quasar sample between redshift 0.8 and 2.2. *MNRAS*, 499(1):210–229, nov 2020.
[94] H. du Mas des Bourboux et al. The Completed SDSS-IV Extended Baryon Oscillation Spectroscopic Survey: Baryon Acoustic Oscillations with Lyα Forests. *ApJ*, 901(2):153, oct 2020.
[95] F. Beutler et al. The 6dF Galaxy Survey: baryon acoustic oscillations and the local Hubble constant. *MNRAS*, 416(4):3017–3032, oct 2011.

[96] C. Blake et al. The WiggleZ Dark Energy Survey: joint measurements of the expansion and growth history at z ¡ 1. *MNRAS*, 425(1):405–414, sep 2012.
[97] DES Collaboration. Dark Energy Survey Year 1 Results: Measurement of the Baryon Acoustic Oscillation scale in the distribution of galaxies to redshift 1. *MNRAS*, 483(4):4866–4883, mar 2019.
[98] DES & SPT Collaborations. Dark Energy Survey Year 1 Results: A Precise H_0 Estimate from DES Y1, BAO, and D/H Data. *MNRAS*, 480(3):3879–3888, nov 2018.
[99] DES Collaboration. Dark Energy Survey Year 3 results: A 2.7% measurement of baryon acoustic oscillation distance scale at redshift 0.835. *Physical Review D*, 105(4):043512, feb 2022.
[100] DES Collaboration. Dark Energy Survey: A 2.1% measurement of the angular baryonic acoustic oscillation scale at redshift $z_{eff} = 0.85$ from the final dataset. *Physical Review D*, 110(6):063515, sep 2024.
[101] S. Sridhar et al. Clustering of LRGs in the DECaLS DR8 Footprint: Distance Constraints from Baryon Acoustic Oscillations Using Photometric Redshifts. *ApJ*, 904(1):69, nov 2020.
[102] R. C. Keenan, A. J. Barger and L. L. Cowie. Evidence for a ~300 Megaparsec Scale Under-density in the Local Galaxy Distribution. *ApJ*, 775(1):62, sep 2013.
[103] M. Haslbauer, I. Banik and P. Kroupa. The KBC void and Hubble tension contradict ΛCDM on a Gpc scale - Milgromian dynamics as a possible solution. *MNRAS*, 499(2):2845–2883, oct 2020.